공학박사 학위논문

Fabrication of Plasmonics Platform for the Chemical and Environmental Sensors

화학 및 환경 센서를 위한
플라즈모닉스 기반의 센서플랫폼 제조

2013 년 8 월

서울대학교 대학원

화학생물공학부

이 수 승

Abstract

Fabrication of Plasmonics Platform for the Chemical and Environmental Sensors

Suseung Lee

School of Chemical and Biological Engineering

The Graduate School

Seoul National University

In the various field of nanotechnology and nanoscience, such as biomedical and environmental science, the design and synthesis of certain nanostructure for a desired purpose is important. Metallic nanostructures have attracted significant attention in the research area of chemical and environmental sensor due to the superior physic-chemical properties and, especially, applicability to the utilization of surface plasmon resonance phenomena.

This thesis mainly deals with the application of novel metallic nanostructures to the surface plasmon resonance phenomena for the realization of effective chemical and environmental sensor. And more detailed strategies and results related with these topics, as follows;

Firstly, highly selective detection system for Cu^{2+} ions by exploiting specific interactions between the Cu-demetallated form (E,Zn-SOD1) of Cu/Zn-superoxide dismutase (SOD1) and Cu^{2+} ions using surface plasmon resonance spectroscopy (SPRS) was suggested. I demonstrated that Cu^{2+} ions have a high affinity for vacant metal-binding sites in the E,Zn-SOD1 protein, compared to other divalent metal ions. On the basis of these measurements, it can be concluded that small amounts of Cu^{2+} ions can be readily detected as the result of the selective binding between the E,Zn-SOD1 protein and Cu^{2+} ions. It appears that metalloproteins have considerable potential for use as a novel sensing actuator, as evidenced by the selective binding of E,Zn-SOD1 proteins with Cu^{2+} ion. This approach can be used in conjunction with other fully or partially demetallated metalloproteins, hence it could be potentially useful in the determination of specific metal ions in aqueous media or demetallated proteins in biological fluids.

Additionally, the applicability of gold nanoparticles as a ratiometric sensor was suggested. From the theoretical study using discrete dipole

approximation method, it is investigated that dimer structure of gold nanoparticles has unique optical properties compared to separated single gold nanoparticle. It can be appeared new plasmon band with longer wavelength due to the electron oscillations along the longitudinal interparticle axis, and this band can be distinguished clearly with the inherent plasmon band. The intensity ratio of inherent and additional plasmon band could be utilized as the value for the ratiometric sensor.

Finally, simple method to fabricate highly branched gold nanostructures with abundant petal-shaped tips by direct growth on the substrate was suggested. A lot of experiments and theoretical calculations have shown highly enhancement of the electromagnetic field in complex gold nanostructures due to the abundant ‘hot spots’ in the individual nanostructures. Among them, multi-branched nanostructure has attracted much attention because of their stronger SERS enhancement factor than other gold nanostructures. In this work, I synthesized and characterized the multi-branched gold nanoparticles, which are applicable to the surface-enhanced Raman detection. It was directly grown on the substrate with simple seed-mediated method, and the optical properties as growth procedure was investigated for the better understanding on the growth process. The multi-

branched gold nanoparticles show the very high enhancement factor, thus it can be promising materials for the effective SERS substrate.

Keywords: Surface plasmon resonance, Ratiometric sensor, Discrete dipole approximation, Biomimetic sensor, Metalloprotein, Metallic nanostructure, Surface enhanced Raman spectroscopy

Student Number: 2008-30894

Contents

List of tables

List of figures

Chapter 1. Introduction

1.1 Surface plasmon resonance (SPR)

The surface plasmon resonance (SPR) means a coherent oscillation of the surface conduction electrons excited by electromagnetic radiation, which can be generally supported with materials that have negative real and positive imaginary part in dielectric constant. [1]

There are two types of SPR transducing mechanism;

(1) Propagating surface plasmon resonance (PSPR)

(2) Localized surface plasmon resonance (LSPR)

Propagating surface plasmons are evanescent electromagnetic waves which are bounded by flat surfaces on the metal-dielectric and arise from oscillations of the conduction electrons in the metal. And localized surface plasmon resonance is observed when the surface plasmons are confined on the nanostructures, which leads to highly localized electromagnetic fields around the nanostructures. Both PSPR and LSPR are sensitive to the local refractive

index changes that occur when the target analyte binds to the metal film or nanoparticles. [2]

Figure 1-1 describes the schematic diagrams of the propagating and localized surface plasmons. The interaction between the metal surface-confined electromagnetic wave and a molecular surface layer of interest induces to change of the plasmon resonance condition, which can be observed with the angle resolved, wavelength shift, and imaging mode. [1, 3-19]

In the first two modes, one measures the reflectivity of light from the metal surface as a function of either angle of incidence (at constant wavelength) or wavelength (at constant angle of incidence). The third method uses light of both constant wavelength and incident angle to interrogate a two-dimensional region of the sample, mapping the reflectivity of the surface as a function of position. [1]

In the localized surface plasmon resonance, incident light interacts with small particles less than the length of incident wavelength (Figure 1-1 (b)). This induces the oscillation of a plasmon locally around the nanoparticle. Both PSPR and LSPR are sensitive to the changes of local dielectric properties in environment, consequently, the changes in the local environment can be investigated through an LSPR wavelength-shift measurement. [1, 2]

(a)

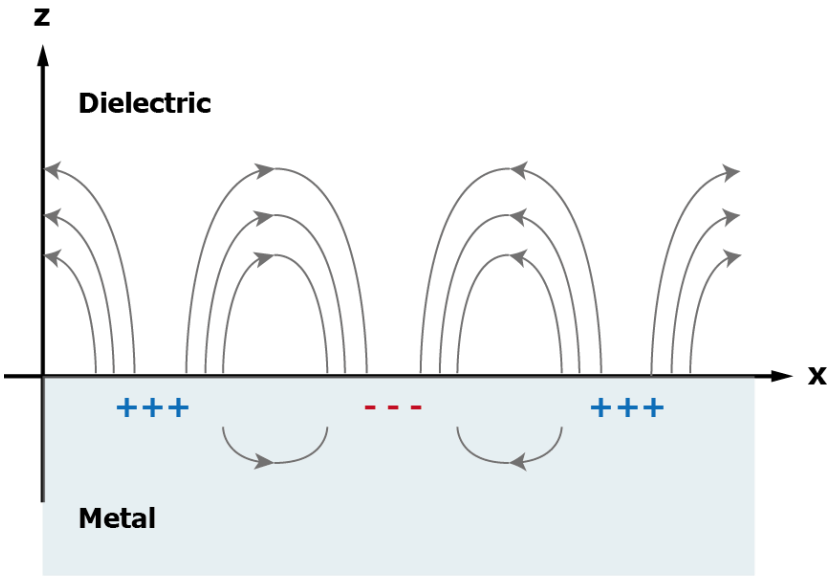

(b)

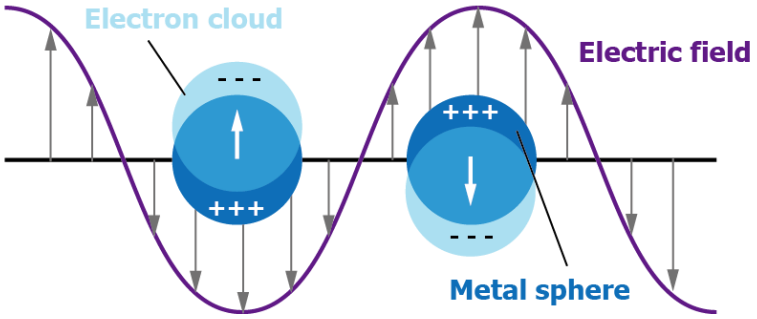

Figure 1-1 Schematic diagrams demonstrating (a) a propagating surface plasmon and (b) a localized surface plasmon. (reprinted from [1])

1.2 Surface-enhanced Raman spectroscopy

Raman scattering is an extremely inefficient process, thus only a small fraction of inelastic scattering which render the Raman spectrum can be observed. The cross sections of Raman scattering are extremely small, which is about 14 orders of magnitude smaller than that fluorescent dye molecules. This means that the detection sensitivity of Raman spectroscopy is intrinsically low and, in order to achieve the high sensitivity required in biological or pollutant samples, the scattering intensity should be greatly increased. [20]

Despite the extremely low scattering intensity, when the molecules are located in the vicinity of a metal nanoparticle or a roughened metallic surface, the Raman cross section can be amplified dramatically. This enhancement effect is known as surface enhanced Raman scattering or surface enhanced Raman spectroscopy (SERS). SERS is probably one of the most powerful techniques currently available for sensing applications since, additionally to an extremely high sensitivity; it provides valuable structural information on the analyzed molecule. [20-40]

It is widely known that there are two enhancement mechanisms which contribute to the enhancement effect; electromagnetic mechanism and the chemical mechanism.

Especially in the electromagnetic mechanism, localized electric fields around the metal nanoparticle are amplified due to the surface plasmon excitation. This induces more intense electronic transitions at the molecules located on the nanoparticle, and consequently enhances Raman scattering. Electromagnetic mechanism plays a major role when compared to the chemical mechanism. Moreover, higher SERS enhancements can be obtained by optimizing the optical properties of the metallic nanoparticles. [20]

1.3 Objectives

In the field of nanoscience, biomedical, environmental science and catalysis, the design and synthesis of certain nanostructure for desired purpose is important. Especially, metallic nanostructures have attracted significant attention in the field of chemical and environmental sensor due to the superior physic-chemical properties and applicability to the utilization of surface plasmon resonance phenomena. The objectives of this thesis are the application novel metallic nanostructures with the surface plasmon resonance phenomena for the realization of effective chemical and environmental sensor.

The detailed objectives are summarized as follows;

(1) To develop the detection system for certain metal ions using surface plasmon resonance spectroscopy (SPRS). In particular ‘selectivity’ was focused on, and partially demetallated metalloprotein was utilized as a sensing actuator for selective detection of copper ion.

(2) To evaluate the applicability of gold nanoparticles as a ratiometric sensor from the theoretical study. Optical properties for dimer structure of gold nanoparticles were estimated using discrete dipole approximation method.

(3) To fabricate the highly branched gold nanostructures with abundant petal-shaped tips by direct growth on the substrate. Multi-branched nanostructure has attracted much attention because of their stronger SERS enhancement factor due to the abundant ‘hot spots’ in the individual nanostructures.

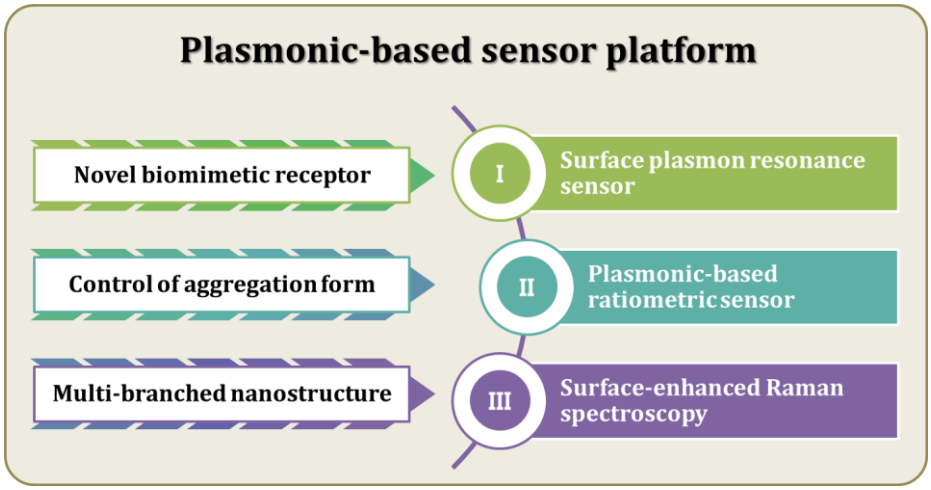

Figure 1-2 Representative diagram for overall objectives of the thesis.

Chapter 2. Biomimetic Sensor Chip for the Surface Plasmon Resonance

2.1 Highly selective detection of Cu^{2+} utilizing specific binding between Cu-demetallated superoxide dismutase 1 and Cu^{2+} ion via surface plasmon resonance spectroscopy

The selective recognition of the specific material, i.e., the development of a highly selective sensing system, is a very important issue for many areas of science and engineering. [41-45] The precise and accurate detection of metal ions is particularly important, since they can have detrimental effects on humans and the environment. A variety of analytical tools have been developed using separation methods, spectroscopic methods, electroanalytical methods, and related techniques. Among them, spectroscopic analysis, such as atomic absorption spectrometry (AAS), inductively coupled plasma atomic emission spectroscopy (ICP-AES) and inductively coupled plasma mass spectrometry (ICP-MS), are currently in widespread use, because they can be qualitatively and quantitatively used to analyze a specific metal ion. However,

there are some limitations to their accuracy due to chemical / physical interference or spectral interference resulting from similarities in coexisting metal ion species. [46]

I report herein on the highly selective detection system for Cu^{2+} ions by exploiting specific interactions between the Cu-demetallated form (E,Zn-SOD1) of Cu/Zn-superoxide dismutase (SOD1) and Cu^{2+} ions using surface plasmon resonance spectroscopy (SPRS). It is well known that metalloproteins contain specific binding sites for certain metal ions. [47] The SOD1 protein is also a type of metalloprotein (figure 2-1). Specifically, it is a metalloenyme that contains Cu and Zn as metal cofactors which function differently. [48-50] Cu is directly involved in the catalytic activity of the enzyme, while Zn stabilizes the conformation of the protein. [51] Therefore, it is reasonable to assume that E,Zn-SOD1 protein contains the specific site, where a Cu^{2+} ion selectively binds, thus maintaining its structure due to the role of Zn in its structure, as shown in the description in figure 2-2. To further investigate this issue, I utilized E,Zn-SOD1 protein as a material that recognizes Cu^{2+} ions and measured the specific interactions of Cu^{2+} ions with the protein, compared with other divalent metal ions.

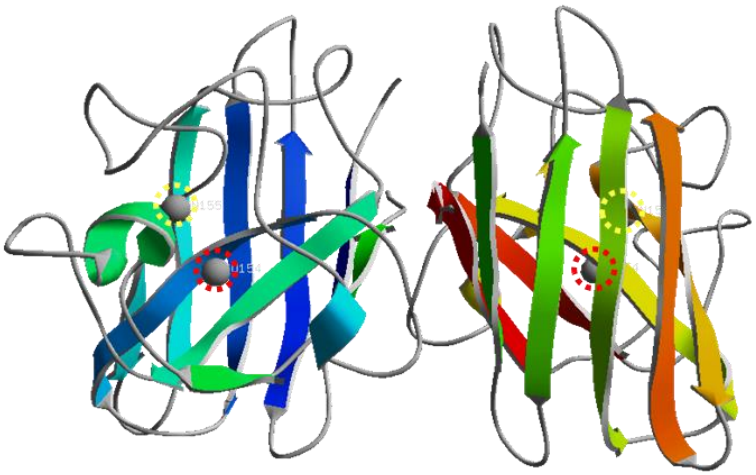

Figure 2-1 A schematic diagram of Cu/Zn-superoxide dismutase. They were made with PDB file (code; 1SPD) from Protein Data Bank (http://www.rcsb.org) by Swiss PDB viewer

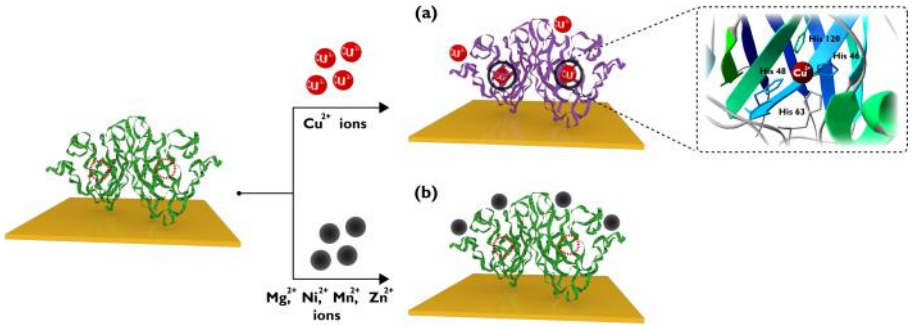

Figure 2-2 Schematic representation of incorporation and binding of Cu^{2+} ions to the vacant metal-binding sites of the E,Zn-SOD1 proteins immobilized on gold thin layer; There are two vacant metal-binding sites in an E,Zn-SOD1 protein originally. (a) Cu^{2+} ions can incorporate and bind into those vacant sites as shown in a magnified description. It shows the coordination structure around a Cu^{2+} ion, when Cu^{2+} ion is incorporated in the E,Zn-SOD1 protein.; (b) Other divalent ions do not bind strongly into vacant sites due to the poor coordination ability in E,Zn-SOD1 protein.

2.2 Materials and Experiments

2.2.1 Materials

E,Zn-SOD1 proteins was purified and purchased from Abfrontier (Korea). 11-Mercaptoundecanoic acid (MUA, 95%, Aldrich), N-hydroxysuccinimide (NHS, 98%, Aldrich), N,N-(3-dimethylaminopropyl)-N′-ethyl-carbodiimide hydrochloride (EDC, ≥99%, Sigma), copper(II) sulfate pentahydrate (≥98%, Sigma-Aldrich), zinc sulfate heptahydrate (99%, Sigma-Aldrich), nickel(II) sulfate hexahydrate (99%, Sigma-Aldrich), magnesium sulfate heptahydrate (≥98%, Sigma-Aldrich), manganese(II) sulfate monohydrate (≥98%, Sigma-Aldrich) were purchased and used without any further pretreatment. Commercial SOD assay kit was purchased from Dojindo Molecular Technologies.

All glassware were cleaned by soaking in piranha solution (98% H_2SO_4 : 30% H_2O_2 = 7:3 v/v) for 60 minutes, and copiously rinsed with deionized water and ethanol, and dried in the oven at a temperature of 65℃.

2.2.2 Preparation of E,Zn-SOD1 protein

To prepare the E,Zn-SOD1 protein, Human SOD1 genes encoding the wild type were cloned into the pET23b(+)(Novagen) vector. The proteins were expressed in E. coli BL21(DE3)pLysS followed by demetallization of SOD1 and re-metallization with Zn^{2+} ions. [52]

2.2.3 Preparation of proteins-immobilized SPR sensor chip

E,Zn-SOD1 proteins were immobilized on a thin gold film. A 50-nm gold thin film was evaporated on a BK7 glass block, and then treated with an 11-mercaptoundecanoic acid (MUA) solution to produce a self-assembled layer. The carboxyl acid groups on the MUA layer were activated by means of the N-hydroxysuccinimide (NHS) / N,N-(3-dimethylaminopropyl)-N′-ethyl-carbodiimide hydrochloride (EDC) coupling procedures. [53]

Finally, E,Zn-SOD1 proteins were exposed to the functionalized SPR chip for 1 hour, and rinsed with deionized water repeatedly.

2.2.4 The enzymatic activity of superoxide dismutase proteins

The enzymatic activity of the E,Zn-SOD1 protein after treatment with the Cu^{2+} solution was determined using a commercial SOD assay kit (Dojindo Molecular Technologies) in conjunction with UV-Vis spectrophotometry (figure 2-3).

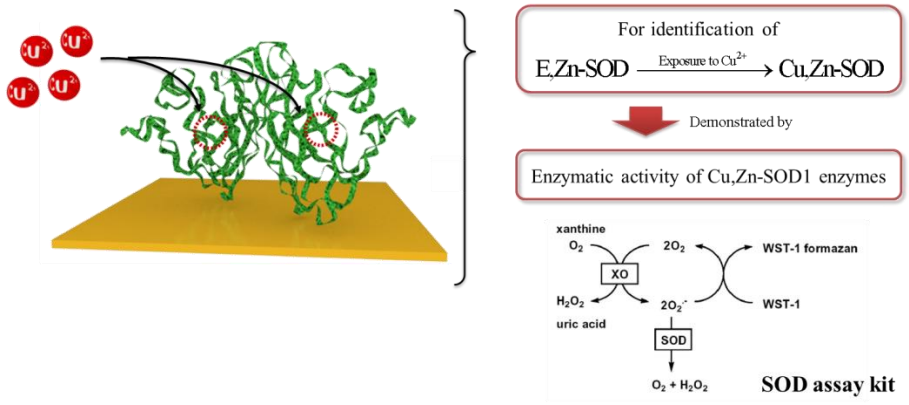

Figure 2-3 The schematic diagram of the enzymatic activity analysis of the E,Zn-SOD1 protein after treatment with the Cu^{2+} solution using a commercial SOD assay kit.

2.3 Results and discussion

SPRS analyses were carried out for Cu^{2+} and four other divalent metal ions (Mg^{2+}, Ni^{2+}, Mn^{2+} and Zn^{2+}) to check possible inherent interferences in the SPRS system which could occur, because these ions are of similar sizes and have similar outer electron configurations. The immobilized E,Zn-SOD1 proteins were exposed to 1 mM solutions of each divalent metal with a 2 μl/min volumetric flow rate for 20 min. After exposure to Cu^{2+} ions, they were washed extensively with deionized water, and the SPR reflectivity at a fixed angle was measured throughout the entire process. As shown in figure 2-4, Cu^{2+} ions induced a significant increase in SPR reflectivity, whereas the other divalent metal ions did not. The experiment with the mixture solution contained various divalent metal ions was performed and the same result was obtained. (figure 2-5) This finding suggests that the E,Zn-SOD1 protein selectively recognizes Cu^{2+} ion compared to the other divalent metal ions, since the E,Zn-SOD1 protein has a specific vacancy for coordination with Cu^{2+} ion.

In order to further validate this conclusion, I tested the enzymatic activity of the E,Zn–SOD1 protein after exposure to a Cu^{2+} solution. The enzymatic activity of the E,Zn-SOD1 protein after treatment with the Cu^{2+} solution was determined using a commercial SOD assay kit (Dojindo Molecular

Technologies) in conjunction with UV-Vis spectrophotometry. [54] A 2.0 μg/ml sample of the E,Zn-SOD1 protein was treated with a 10 μM Cu^{2+} ion solution, and the assay was performed. As shown in the data in figure 2-6 (a) and (b), exposure to the Cu^{2+} ion solution led to a significant increase in the enzymatic activity of the E,Zn-SOD1 protein. The normalized enzymatic activity increased up to 66.7 %, double the enzymatic activity found before exposure. The result of a control test (figure 2-6 (c)) shows that free Cu^{2+} ions in solution do not affect the activity measured by an assay kit, and these results suggest that the increase in enzymatic activity after exposure to the Cu^{2+} ion solution is clearly due to the recovery of activity, as the result of the transformation of E,Zn-SOD1 to the fully-metallated form (Cu,Zn-SOD1). Collectively, I conclude that the E,Zn-SOD1 protein selectively recognizes Cu^{2+} ion and that its enzymatic activity is recovered on the incorporation and binding of a Cu^{2+} ion to the vacant site of the E,Zn-SOD1 protein.

Having established that the E,Zn–SOD1 protein has a strong affinity toward Cu^{2+} ion and that it can selectively detect Cu^{2+} ion over other metal ions, I also evaluated the sensitivity of the system. Various concentrations of Cu^{2+} ion solutions in the range of 10 to 100 μM were tested. SPR plots (R-θ plots) were collected before and after a 1 h-exposure to each concentration of Cu^{2+} ion solution. As shown in figure 2-7, the SPR angle dramatically

increased at a concentration of 40 μM Cu^{2+} ion solution and showed a linear response to a 100 μM concentration. This is due to the changes in dielectric property around the gold thin film which is induced by incorporation of Cu^{2+} ions by E,Zn-SOD1 proteins. Generally, the extent of change in the SPR angle increases in proportion to change in dielectric properties.

In conclusion, I demonstrate herein that Cu^{2+} ions have a high affinity for vacant metal-binding sites in the E,Zn-SOD1 protein, compared to other divalent metal ions. On the basis of these measurements, it can be concluded that small amounts of Cu^{2+} ions can be readily detected as the result of the selective binding between the E,Zn-SOD1 protein and Cu^{2+} ions. It appears that metalloproteins have considerable potential for use as a novel sensing actuator, as evidenced by the selective binding of E,Zn-SOD1 proteins with Cu^{2+} ion. I believe that this approach can be used in conjunction with other fully or partially demetallated metalloproteins. Consequently, it could be potentially useful in the determination of specific metal ions in aqueous media or demetallated proteins in biological fluids.

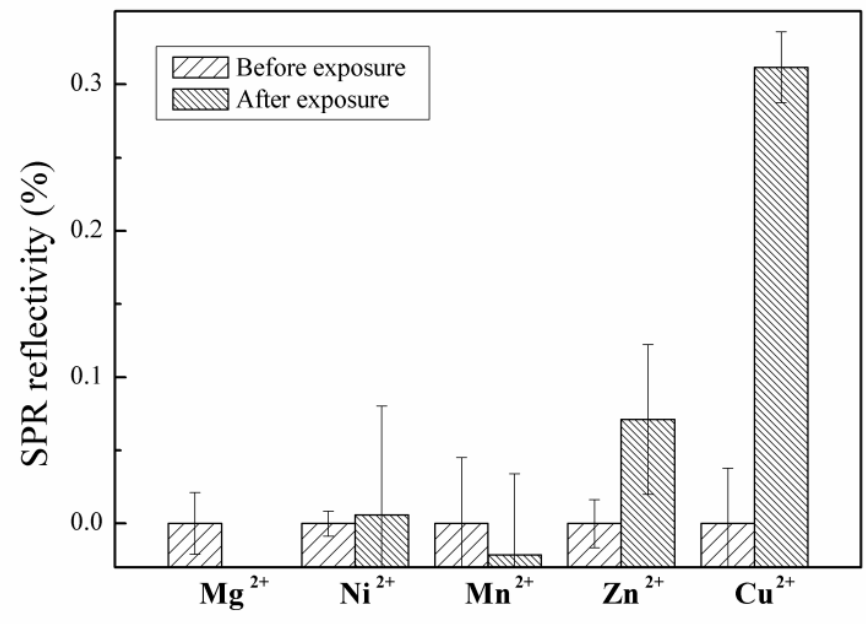

Figure 2-4 SPR reflectivity values at the fixed angle of the lower inflection point in each SPR curve were obtained by averaging each of several values in their stabilized region. All measurements were normalized by setting the SPR reflectivities obtained before exposure to zero; before (sparse-patterned bars) and after (dense-patterned bars) exposure to 1 mM of five divalent metal ions. An error-bar means standard deviation for collected SPR reflectivities in their stabilized region. Exposure to divalent metal ions was performed for 20 min.

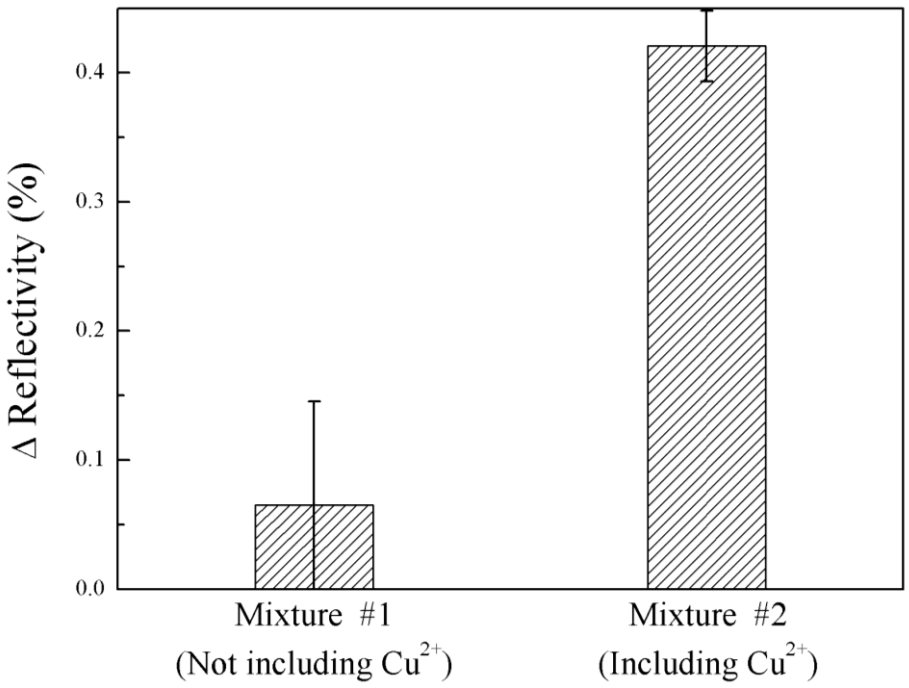

Figure 2-5 Selectivity test in mixed metal ion solutions; SPR reflectivity values at the fixed angle of the lower inflection point in each SPR curve were obtained by averaging each of several values in their stabilized region. ΔReflectivity means the difference of SPR reflectivity between before and after exposure to each mixture. ('Mixture #1' solution is a mixture of 10 mM equivalent Mg^{2+}, Ni^{2+}, Mn^{2+} and Zn^{2+} solution. 'Mixture #2' contained the same concentration and equivalent Cu^{2+} solution.)

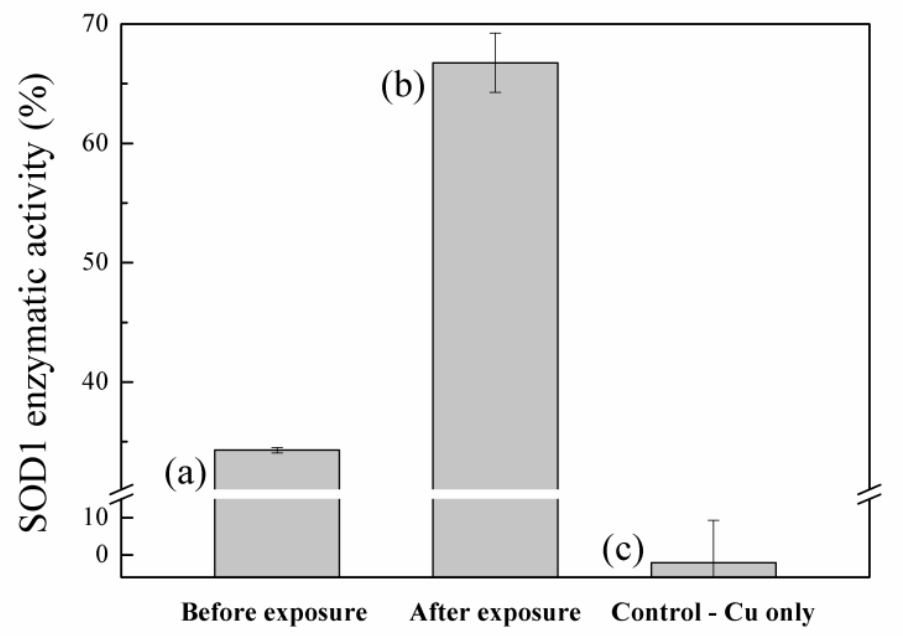

Figure 2-6 The enzymatic activity of superoxide dismutase proteins measured using a commercial SOD assay kit (a) before and (b) after exposure to a 10 μM solution of Cu^{2+} ions with 2 μg/ml of E,Zn-SOD1 proteins. (c) Enzymatic activity for 10 μM of Cu^{2+} ions solution without E,Zn-SOD1 proteins (as a control).

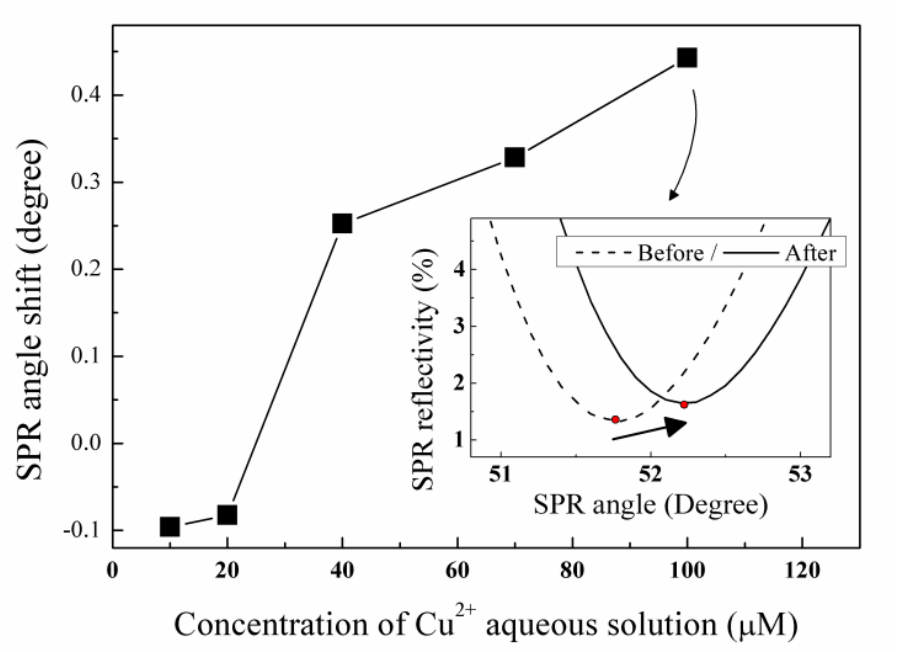

Figure 2-7 Calibration curve of absolute changes in SPR angle versus exposure concentration of Cu^{2+} ions. Inset indicates typical SPR plots before (dashed line) and after (solid line) exposure to 100 μM of Cu^{2+} ions solution. Exposure to divalent metal ions was performed for 1 hour.

Chapter 3. Plasmonic-based ratiometric sensor

3.1 Theoretical study for the plasmonic-based ratiomety sensor

Optical spectroscopy, such as UV-visible and fluorescence spectroscopy, is widely used for the quantitative or qualitative analysis in the various field of research. However most optical spectroscopy has the major limitation as intensity-based probes, in which variations in the environmental sample. It is well-known that many factors may influence the emission intensity, such as the illumination intensity, optical path length and the concentration of probes, which are prone to be disturbed in quantitative detection. From this point of view, the concept of ratiometric sensor may be an attractive choice, because that ratiometric measurements have the important feature that they permit signal rationing, and thus increase the dynamic range and provide built-in corrections for environmental effect. [55-57]

Although many research related to the ratiometric sensor have been studied, most researches were focused on the utilization of fluorescence probe [56, 58-61] using intramolecular charge transfer (ICT) [62-66], fluorescence

resonance energy transfer (FRET) [67-70] and monomer-excimer transformation [71, 72].

Metallic nanoparticles are well known as promising sensing probe compared to the organic materials. Although they have superior optical properties such as large light absorption / scattering cross-section [73, 74] and physic-chemical stability, there were almost no researches related with the ratiometric sensor using metallic nanoparticles. It is because that the metallic nanoparticles with typical shape mostly have one surface plasmon resonance (SPR) band, thus it is difficult to utilize two or more band for signal rationing.

Almost researches related with optical sensors using metallic nanoparticles have been utilized the spectral changes from random aggregation induced by the analyte. However such a random aggregation of metallic nanoparticles usually generates a broaden band which cannot be quantified. It is because that numerous kinds of aggregate form with different size and shape make the ensemble-averaged spectrum.

In this work, I suggested that the applicability of gold nanoparticles to ratiometric sensor by preventing random aggregation of the nanoparticles. Two-touching nanostructure, dimer structure, which induced by limited aggregation can generate an extra characteristic band that can be quantified

clearly, due to the absence of ensemble average effect. Thus, it is expected that by rationing the intensity of inherent and new generated SPR bands, gold nanoparticles can be applied to the ratiometric sensor. As theoretical evidence, optical properties of for the dimer structure of gold nanoparticle were calculated and compared to that of separated single gold nanoparticles.

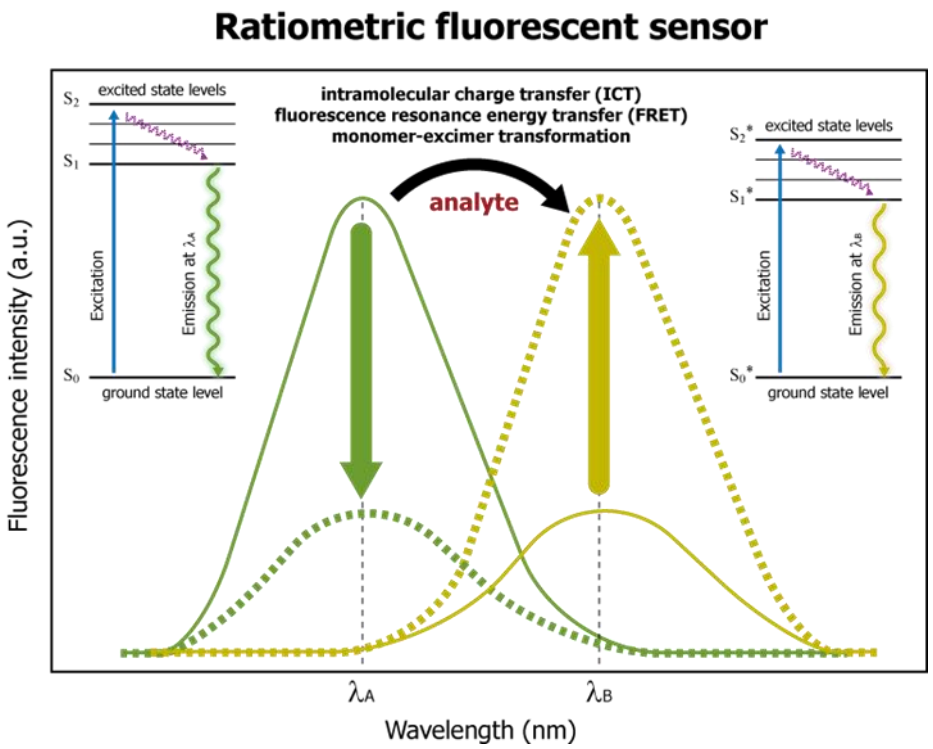

Figure 3-1 Schematic diagram for the principle of ratiometric fluorescent sensor

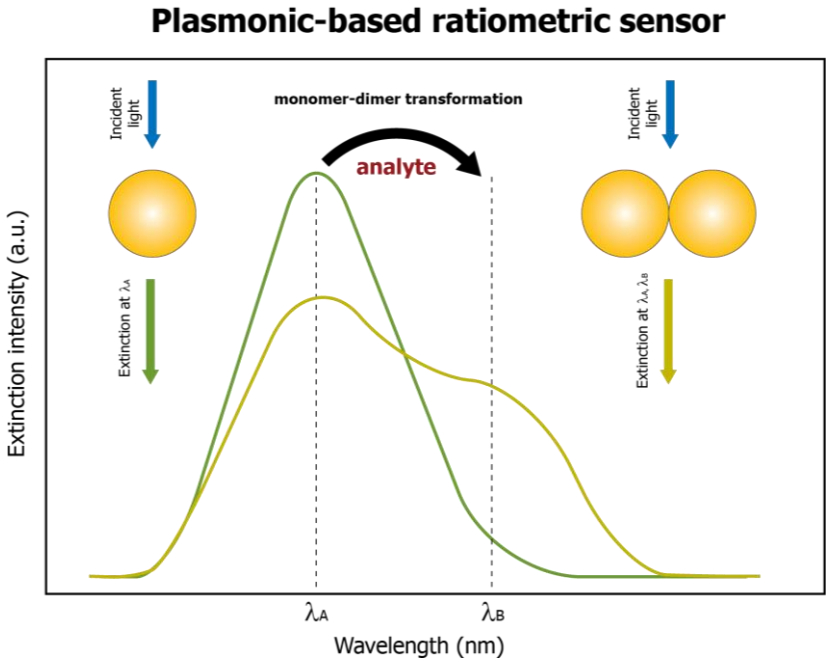

Figure 3-2 Schematic representation of the gold nanoparticle –based ratiometric sensor by limited aggregation.

3.2 Theoretical calculation of the optical properties

Optical properties, such as absorption, scattering and extinction spectra, of single and dimer-structure gold nanoparticle was calculated using the discrete dipole approximation (DDA) method [75].

All DDA calculations were solved using DDSCAT 7.2 code, which was developed by Drain and Flatau [76]. For the calculation, the dielectric constants of gold were obtained from the literature.

3.3 Results and discussion

Extinction coefficient of single and dimer-structure of gold nanoparticle with various size was calculated using the discrete dipole approximation (DDA) method [75]. For the calculation, two models for the calculation was generated as followed;

(1) Two gold nanoparticles with $6.67 \times d_{Au}$ nm of interparticle distance

(2) Two gold nanoparticles with 0 nm of interparticle distance (dimer)

Firstly, it was investigated that how the incident polarized direction influences the optical absorption efficiency of dimer structure, the absorption, scattering and extinction spectra for dimer structure. The optical properties of metallic nanoparticles are dominated by the collective oscillation of the conduction electrons resulting from the interaction with incident electromagnetic field. Thus in the case of asymmetric structure, it is important to identify the effect of incident polarized direction. In Figure 3-3, the dimer spectra corresponding to polarization of the input light with various incident angles along the interparticle axis is shown, consistent with excitation of the dimer plasmon. In the case of parallel incident along the interparticle axis, the dimer structure shows the similar spectra with plasmon band at 520 nm to that of typical sphere nanoparticle. However, as the incident angle decreased from

90° to 0°, another plasmon band at 580 nm appear and gradually increase. SPR wavelength remains unchanged corresponding to the incident angles, but intensity ratio of inherent band to another band changed. Finally, in the case of perpendicular incident along the interparticle axis, intensity of new generated plasmon band increased than that of inherent plasmon band. (figure 3-4) Furthermore, it was investigated the size effect of gold nanoparticle to the optical properties of separated and dimer structure. Each structure with 15-nm, 30-nm and 50-nm of gold nanoparticle were studied. All calculation were performed with seven different angle of incident light, from 0° ~ 90°, and averaged, due to the asymmetry of dimer structure. As shown in figure 3-5, t is interesting to note that the number of extra peaks at the longer wavelength is increase as the size of gold nanoparticles is larger. This effect may be due to additional multipolar resonances induced by the longitudinal plasmon resonance along the interparticle axis.

And to conclude, in this work, the applicability of gold nanoparticles as a ratiometric sensor was studied by theoretical calculation. Dimer structure of gold nanoparticles has unique optical properties compared to separated single gold nanoparticle. A new plasmon band at loner wavelength was appeared due to the electron oscillations along the longitudinal interparticle axis. Thus if the aggregation of gold nanoparticles induced by analyte can be limited to the

dimer structure, the intensity ratio of inherent and additional plasmon band could be utilized as the value for the ratiometric sensor.

(a)

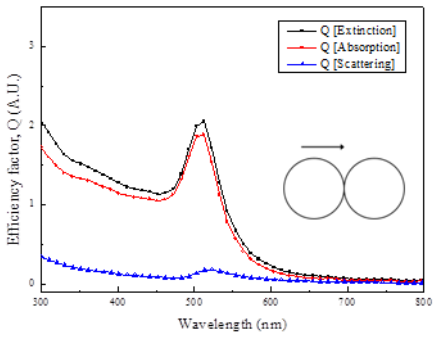
Q [Extinction]
Q [Absorption]
Q [Scattering]
Efficiency factor, Q (A.U.)
Wavelength (nm)

(b)

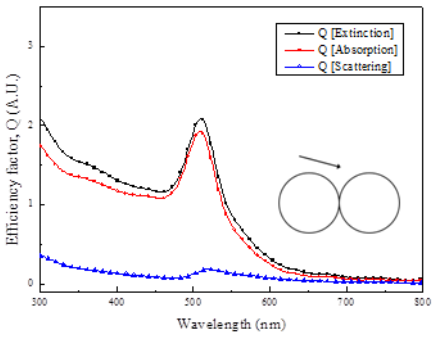
Q [Extinction]
Q [Absorption]
Q [Scattering]
Efficiency factor, Q (A.U.)
Wavelength (nm)

(c)

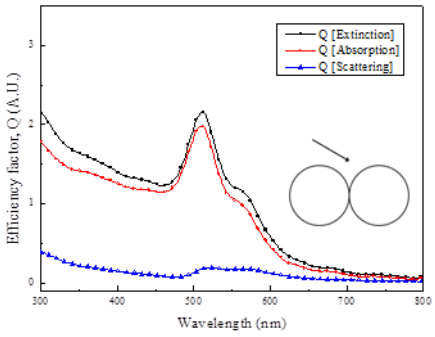
Q [Extinction]
Q [Absorption]
Q [Scattering]
Efficiency factor, Q (A.U.)
Wavelength (nm)

(d)

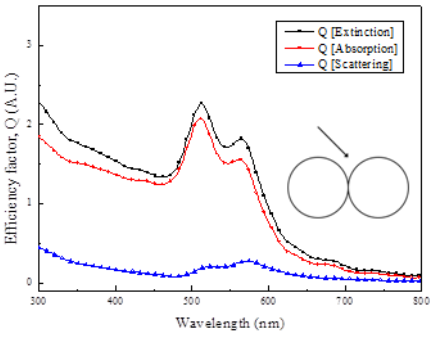
Q [Extinction]
Q [Absorption]
Q [Scattering]
Efficiency factor, Q (A.U.)
Wavelength (nm)

(e)

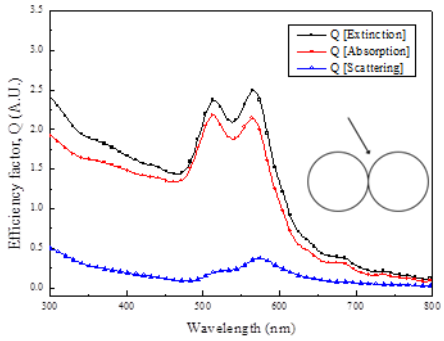

(f)

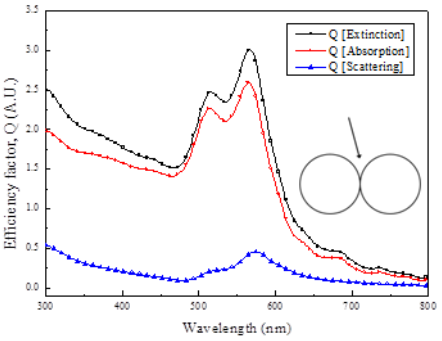

(g)

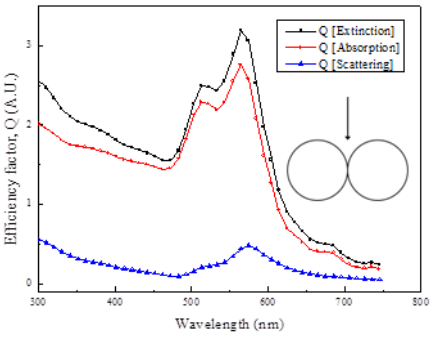

Figure 3-3 Theoretical calculation of the optical properties for Au-Au dimer structure with different light incident angle; (a) 90º, (b) 75º, (c) 60º, (d) 45º, (e) 30º, (f) 15º, (g) 0º

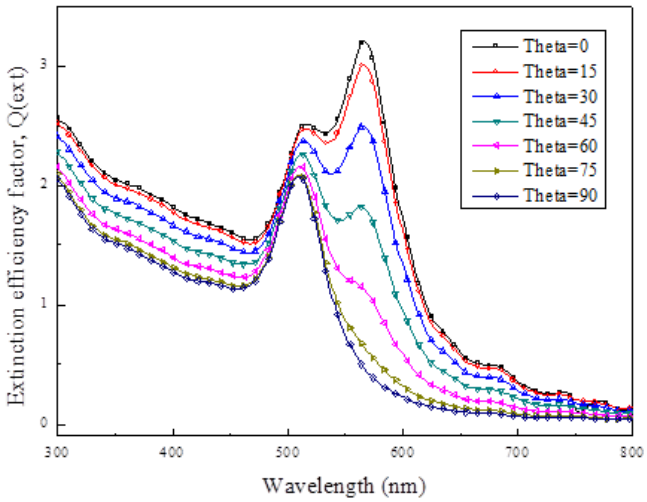

Figure 3-4 Theoretical calculation of the extinction spectrum for Au-Au dimer structure with different incident angle ($0° \sim 90°$)

(a)

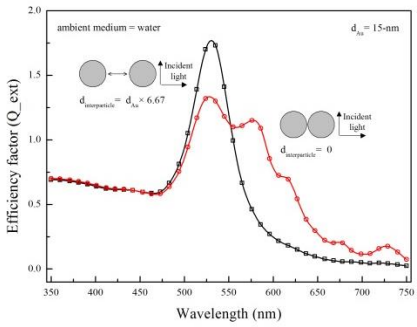

(b)

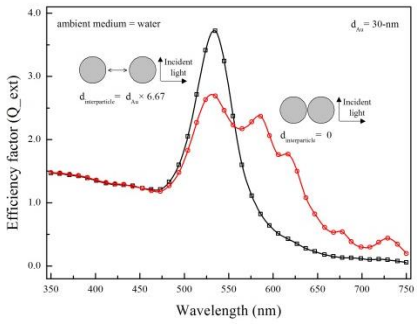

(c)

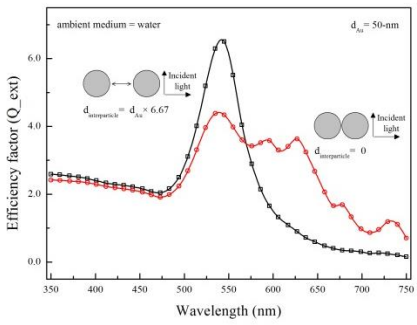

Figure 3-5 Theoretical calculation of the extinction spectrum for Au-Au dimer structure with different size of gold nanoparticles, and comparison to the separated gold nanoparticle.

Chapter 4. Metallic nanostructure for the Surface-enhanced Raman Active Substrate

4.1 Synthesis of multi-branched gold nanoparticles on the substrate and its application to the SERS

Since its discovery more than 30 years ago [77-79], the field of surface-enhanced Raman spectroscopy (SERS) has grown dramatically, demonstrating its power as an analytical tool for the sensitive and selective detection of molecules adsorbed on noble metal nanostructures.

Despite the mechanism of SERS is still a matter of controversy, the enhancement factor, $EF_{SERS} \sim 10^6$, could be understood as the product of two contributions: (a) an electromagnetic enhancement mechanism and (b) a chemical enhancement mechanism [80].

Especially, the electromagnetic enhancement mechanism, an important EF contribution, is closely related with the composition, size and shape of metallic nanostructure. Thus extensive studies have been focused on the development of unique nanostructure with various shape and size. In particular, novel metals such as gold and silver have been intensively

investigated with different morphology such as rod [81-84], star [85-90], flower [91-93] shape.

Experiments and theoretical calculations [94-96] have shown highly enhancement of the electromagnetic field in complex gold nanostructures due to the abundant ‘hot spots’ in the individual nanostructures. Among them, multi-branched nanostructure has attracted much attention because of their stronger SERS enhancement factor than other gold nanostructures. [97]

Herein, I report a simple method to fabricate highly branched gold nanostructures with abundant petal-shaped tips, by direct growth on the substrate. And I investigate the growth procedure of the structure in detail for understanding on the growth process of multi-branched gold nanoparticle.

4.2 Materials and experiments

4.2.1 Materials

Gold(III) chloride trihydrate ($HAuCl_4$, ≥49.0%, Sigma-Aldrich), hexadecyltrimethylammonium bromide (CTAB, ≥98%, Sigma), sodium borohydride (99%, Aldrich), silver nitrate (≥99.0%, Sigma-Aldrich), *L*-ascorbic acid (≥99%, Sigma-Aldrich), (3-Mercaptopropyl)trimethoxysilane (MPTMS, 95%, Aldrich), rhodamine 6G (Rh6G, 99%, Aldrich) were purchased and used without any further pretreatment.

All glassware were cleaned by soaking in piranha solution (98% H_2SO_4 : 30% H_2O_2 = 7:3 v/v) for 60 minutes, and copiously rinsed with deionized water and ethanol, and dried in the oven at a temperature of 65℃.

4.2.2 Preparation of seed nanoparticles and growth solution

Multi-branched gold nanoparticles were synthesized using seed-mediated method.

The solution of seed nanoparticles was prepared by following a previously reported method. [98]

100 µl of 5.0×10^{-2} M $HAuCl_4$ was added to 40 ml of 1.50×10^{-1} M CTAB prepared in a piranha-cleaned 80-ml vial with continuous stirring. Then 2.5 ml of 1.0×10^{-2} M sodium borohydride cooled in an ice bath was added and the color of solution quickly changed to brownish red. After keeping stirring for 2 minutes, solution of seed nanoparticles was successfully synthesized and it was used after storage for 3 hours at room temperature.

Growth solution for the synthesis of branched gold nanoparticle was prepared as followed. 40 ml of 5.0×10^{-2} M CTAB in a piranha-cleaned 80-ml vial with 200 µl of 5.0×10^{-2} M $HAuCl_4$ and 1.2 ml of 7.0×10^{-3} M was prepared, then 300 µl of 1.0×10^{-1} M *L*-ascorbic acid was added. The color of solution changed immediately from dark yellow to colorless, and synthesized growth solution was used freshly made.

4.2.3 Direct growth of branched gold nanoparticles on the glass substrate

Two types of glass substrate were used for the growth of nanostructure; slide glass (76 × 26 × 1 mm, Marienfeld-Superior, German) for the analysis of

dark-field microscopy and cover glass (18×18×0.13~0.16 mm, Marienfeld-Superior, German) for the analysis of Raman spectroscopy. All glass substrate was cleaned with piranha solution (98% H_2SO_4 : 30% H_2O_2 = 7:3 v/v) for 60 minutes, and rinsed with deionized water and ethanol several times and dried with nitrogen gas.

For the functionalization of substrate with mercaptosilane monolayers, cleaned glass substrates were treated with 5 mM MPTMS ethanolic solution for 12 hours at room temperature, then rinsed with absolute ethanol to remove excess molecules and dried with nitrogen gas. The MPTMS-functionalized glass substrates were soaked into the prepared solution of seed nanoparticles for 1 hour at 30℃ for the immobilization of seed nanoparticles, then rinsed with deionized water and dried with nitrogen gas.

Finally, for the growth of seed nanoparticles to the branched nanostructures, seed-immobilized substrates were immersed in growth solution for 5 hours at 30℃. After growth procedure, they were rinsed with deionized water several times and dried with nitrogen gas.

The successfully prepared branched gold nanoparticles on glass substrate were characterized with field-emission scanning electron microscopy (FE-SEM, with electron gun operating 2.00 kV, Supra 55 VP, Carl Zeiss) for the

observation of morphology. Furthermore, the size, composition and atomic structure of the prepared branched gold nanoparticles were analyzed with a high-resolution transmission electron microscopy (HR-TEM, with an accelerating voltage of 300 kV, JEM-3010, JEOL) with an energy dispersive spectroscopy (EDS)

4.2.4 Analysis of localized surface plasmon resonance (LSPR)

Dark-field microscope system, consisting of an Axio observer Z1 inverted microscope equipped with dark-field condenser (Carl Zeiss, Germany) was used for the observation of the Rayleigh scattering images. [99] The source of illumination was halogen lamp with the 100 W power, and the Rayleigh scattering images were directly collected to a color CCD camera.

The spectrum of Rayleigh scattering was collected using a line-imaging spectrometer (Monorai320i, Dongwoo Optron Co., Korea) coupled with a 1024×256 pixel cooled spectrograph CCD camera (Andor Technology PLC, UK) A programmable shutter is mounted internal to an adjustable entrance slit, the width of which is open to keep nanoparticles in the region of interest. Then, the spectrum was acquired via full vertical binning method, meaning that all CCD columns were integrated and displayed as a single spectrum.

4.2.5 Analysis of Raman spectroscopy

The Raman spectrum was collected at ambient temperature using a QE65-Pro-Raman spectrometer (Ocean Optics, Dunedin, FL, USA) with a coupled fiber probe. The laser excitation wavelength was 785 nm (54.4 mW) and beam was focused to a spot size of 158 μm at the substrate. The scattered Raman signal was integrated for 1 second and measured over a spectral range of 0 to 2000 cm^{-1}. For each measurement, it performed at least 5 times with randomly selected region, and collected spectrum was averaged.

For the Raman-active molecules for SERS, rhodamine 6G (Rh6G, figure 4-1) was chosen as an analyte because it has been well characterized by SERS and by resonance Raman spectroscopy. [100] From the various Raman shift of Rh6G (see table 4-1), the band at 1510 cm^{-1} was selected as representative Raman shift due to its strong intensity.

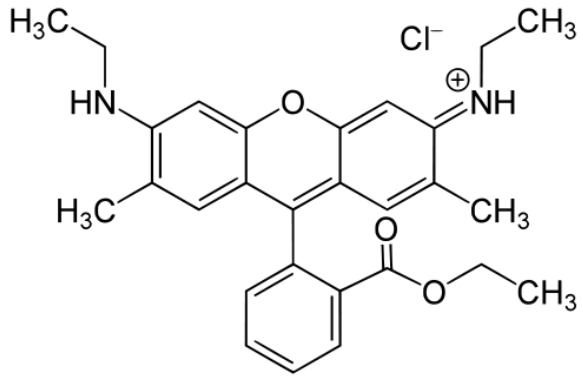

Figure 4-1 Molecular structure of rhodamine 6G;

Table 4-1 Table of Raman shifts for rhodamine 6G [101]

band (cm^{-1})	Assignment
613	C-C-C ring in-plane bending
775	C-H out of plane bending
1185	C-H in-plane bending
1365	aromatic C-C stretching
1510	aromatic C-C stretching

4.3 Results and discussion

Figure 4-2 shows scanning electron microscopy images of as-synthesized particle which consists of many irregular petals. From the analysis with high-resolution transmission electron microscopy, the size of nanostructure is about 200-nm diameter and it is composed of gold only. (figure 4-3 (a),(b)) The lattice fringes with a d-spacing value is 0.24-nm, and it corresponds to the (111) planes of face centered cubic (fcc) gold structure. (figure 4-4 (a),(b))

I should point out that the synthesized multi-branched gold nanoparticles possess several features that can make them suitable for SERS substrates;

(1) Increased surface area due to their roughened surface determined by the tips and the cavities

(2) Contribution to the development of the so called ‘hot spot’ for localized electromagnetic field enhancement.

In order to get a better understanding on the growth process of multi-branched gold nanoparticle, scanning electron microscopy (SEM) analysis were used. As shown in figure 4-3, average size of the nanoparticles was closed up to near 100-nm from 4-nm in 15 minutes (figure 4-5(a)). And as the growth proceeds, petal-like structures develop gradually on the surface of

nanoparticles (figure 4-5(b)-(c)). The final product of synthesized nanoparticles has about 200-nm particle size and many irregular petals on the surface. (figure 4-5(d))

Development of petal-like structures on the surface of gold nanoparticle is due to the large amount of silver ions which commonly employed in the seed-mediated synthesis of gold nanostructure. The reason is unclear at this time, but many research suggest that the under potential deposition of silver toward the surface of the Au nanoparticles can induce the shape-directing effects. [102-104] In fact, with previous study, I investigated that proportion of silver ions causes dramatic changes to the morphology of the products.

The optical properties of the multi-branched gold nanoparticles were investigated by dark-field microscopy measurements at the each step of the synthesis process (figure 4-6 and 4-7). At initial stage of growth procedures within 15 minutes, green-colored scattering spots were generated and developed, which have the localized surface plasmon resonance (LSPR) bands at 540 ~ 580 nm wavelength. This characteristic is similar to the typical single spherical gold nanoparticles. But as the growth proceeds, the color of scattering spots changed from green to red and the brightness increased too. The LSPR bands in this step increased up to near 650 nm wavelength because that multi-branched nanoparticles present several plasmon bands in the NIR

region depending on their symmetry as well as the number and size of their tips [105].

Interestingly, figure 4-8 shows that the LSPR wavelength (λ^{res}_{max}) in the scattering spectra did not changed after growth for 120 minutes, though the scattering intensity at λ^{res}_{max} was still increased consistently. It means that the formation of multi-branched nanostructures are almost completed within 120 minutes, and after that period, only the population of multi-branched gold nanoparticles on the substrate are increased.

In order to investigate the applicability as SERS substrate, rhodamine 6G (Rh6G) was chosen for Raman-active molecules as an analyte, because it has been well characterized by SERS and by resonance Raman spectroscopy. [100]

Intensities of the most Raman shift bands were increased as growth time passed (figure 4-9 and 4-10). Especially the Raman intensity was increased dramatically in the growth procedure within 120 minutes, and it is because that the formation of multi-branched nanostructures is almost completed in that period. Successfully synthesized multi-branched gold nanoparticles show the very high enhancement factor when compared to the cleaned glass substrate. (figure 4-11) They can detect near 1.0×10^{-6} M Rh6G and

distinguish the change of concentration with step-by-step injection. (figure 4-12)

This work reports the synthesis and characterization of multi-branched gold nanoparticles, which are applicable to the surface-enhanced Raman detection. I directly synthesized multi-branched nanoparticles on the substrate with seed-mediated method, and investigated the optical properties as growth procedure for the better understanding on the growth process. The multi-branched gold nanoparticles show the very high enhancement factor, thus it can be utilized as very effective SERS substrate.

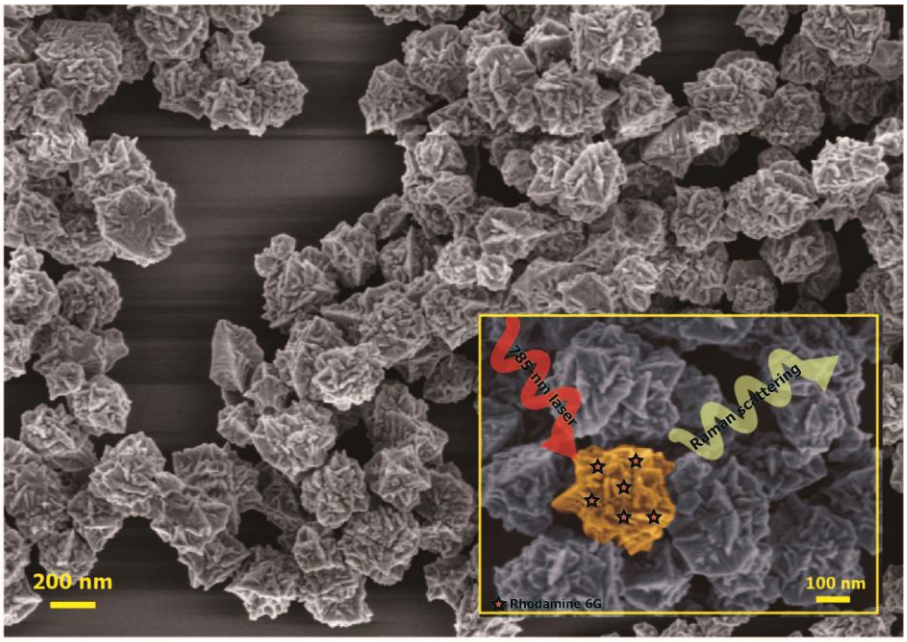

Figure 4-2 Synthesized multi-branched gold nanoparticle, and schematic representation of its application to the surface-enhanced Raman spectroscopy.

(a) (b)

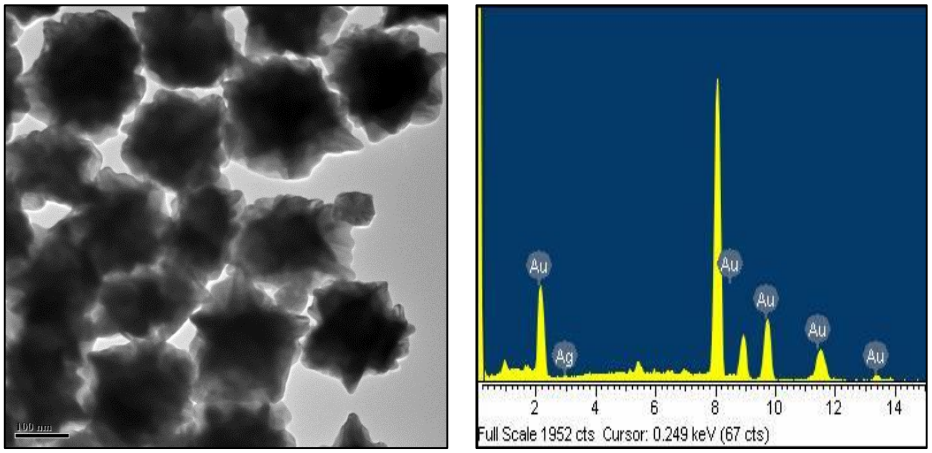

Figure 4-3 TEM analysis of multi-branched gold nanostructures; (a) High-resolution TEM image of synthesized multi-branched gold nanostructures, and (b) EDS spectra of synthesized multi-branched gold nanostructures.

(a) (b)

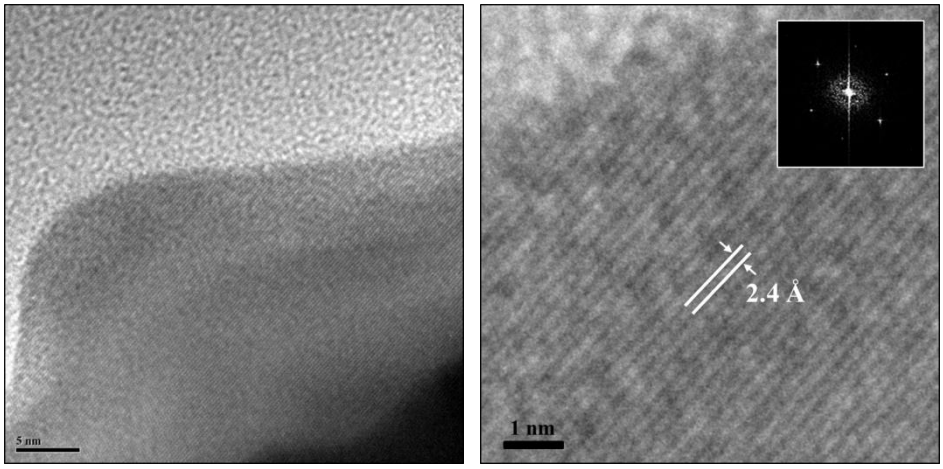

Figure 4-4 High-resolution TEM analysis of multi-branched gold nanostructures; (a) High-resolution TEM image of synthesized multi-branched gold nanoparticle, and (b) Lattice fringes with a d-spacing value of 0.24 nm, which corresponds to the (111) planes of face centered cubic (fcc) gold structure. The inset is FFT pattern of the multi-branched gold nanostructure.

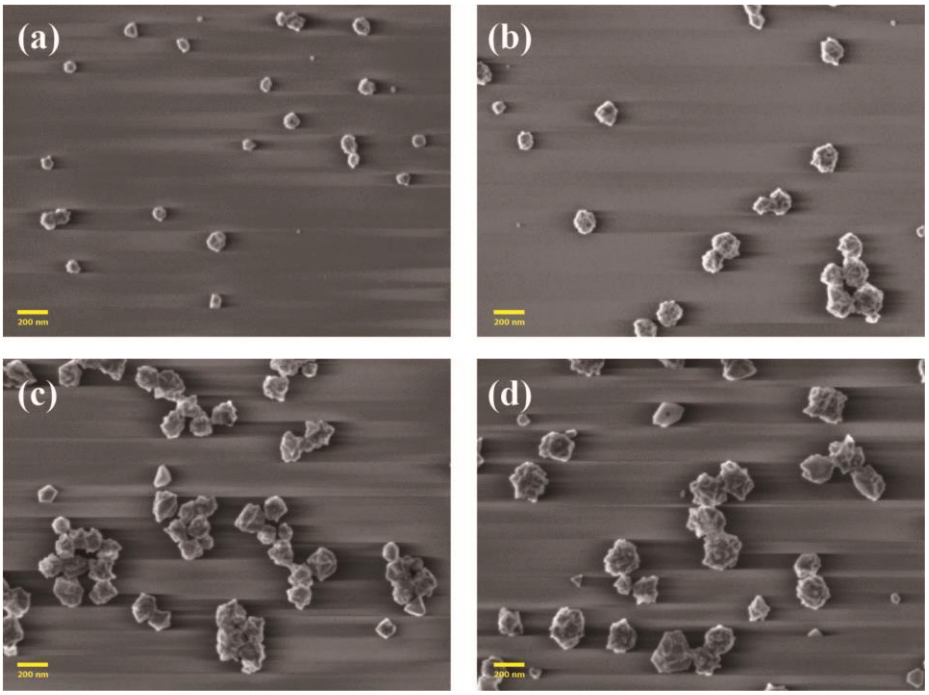

Figure 4-5 Scanning electron microscopy images of synthesized multi-branched gold nanoparticles with respect to growth time; (a) 15 min, (b) 60 min, (c) 120 min, (d) 180 min.

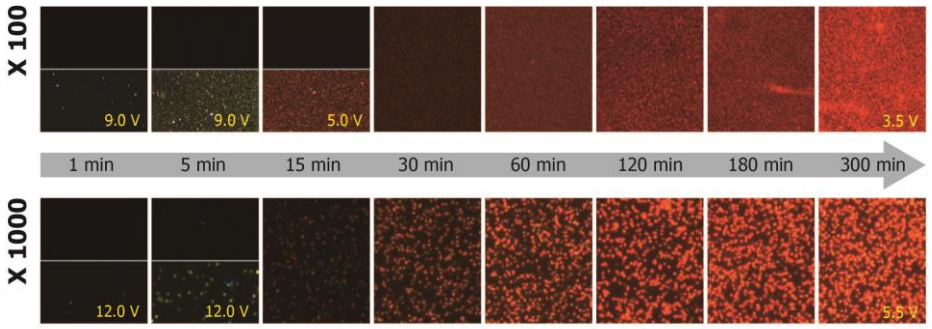

Figure 4-6 Rayleigh scattering images of multi-branched gold nanoparticles with respect to the growth time; Images were collected with ×100 and ×1000 of magnification for the each time, and the power of illumination was constant.

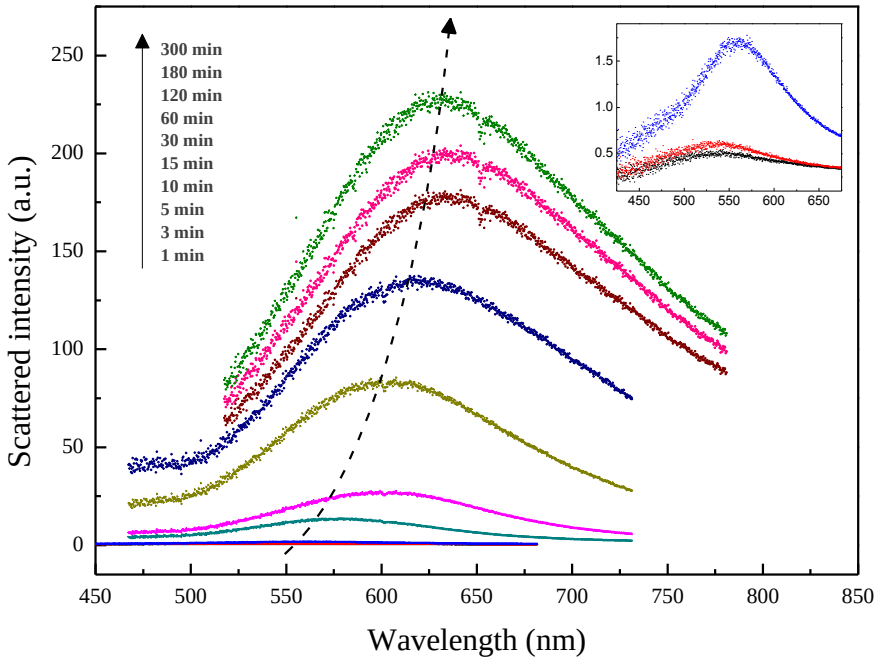

Figure 4-7 Rayleigh scattering spectrum of multi-branched gold nanoparticles with respect to the growth time; each spectrum was collected with full vertical binning (FVB) mode at least 3 times with randomly selected region, and averaged. Inset shows the Rayleigh scattering spectrum of multi-branched gold nanoparticles with 1, 3, 5 minutes of growth time.

(a) (b)

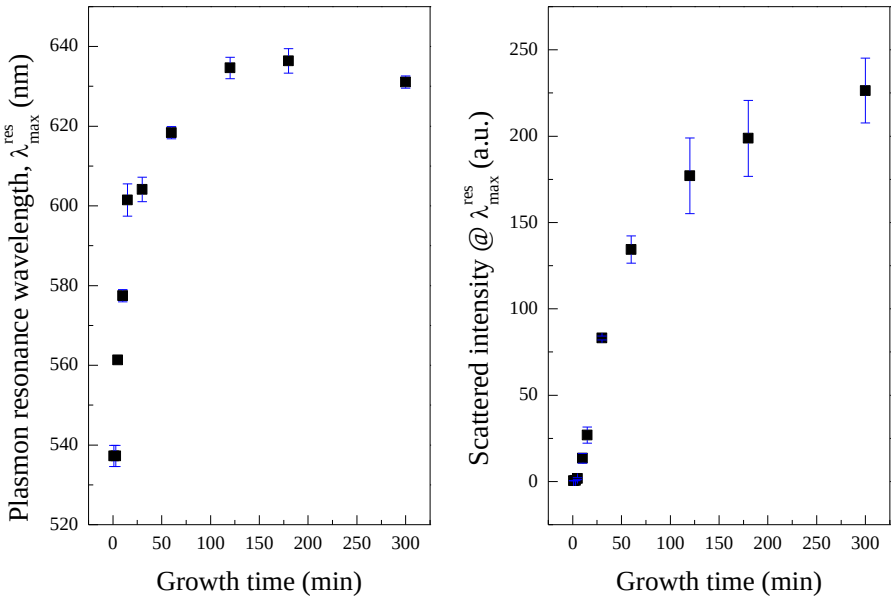

Figure 4-8 (a) Plots of the plasmon resonance wavelength (λ^{res}_{max}) in the scattering spectra, and (b) scattered intensity at λ^{res}_{max} as a function of growth time.

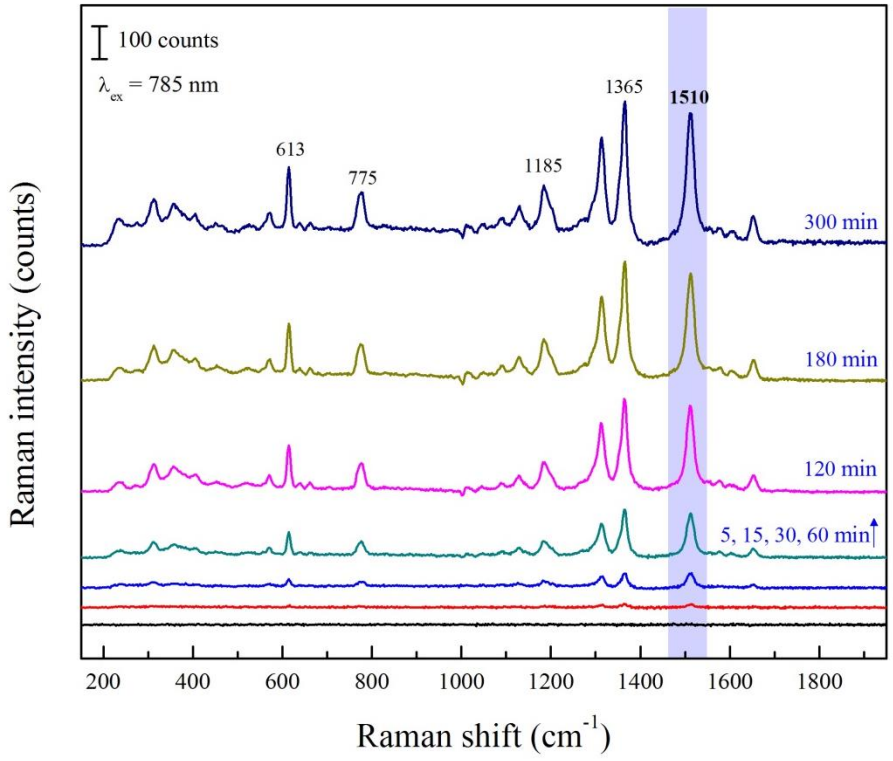

Figure 4-9 Raman spectrum of multi-branched gold nanoparticles with respect to the growth time; each spectrum was collected 9 times with the randomly selected region, and averaged. The wavelength of laser excitation is 785 nm, and integration time is 1 second.

(a)

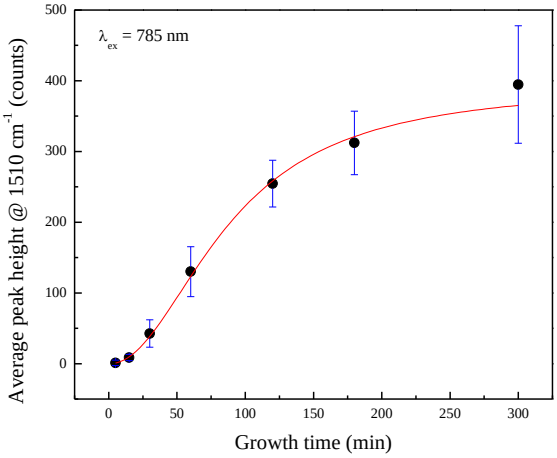
λex = 785 nm
Average peak height @ 1510 cm-1 (counts)
Growth time (min)

(b)

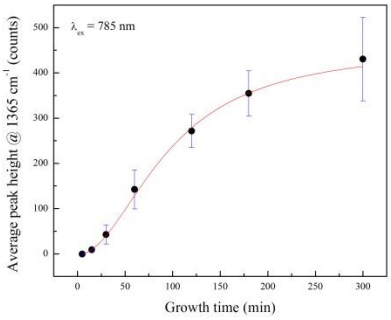
λex = 785 nm
Average peak height @ 1365 cm-1 (counts)
Growth time (min)

(c)

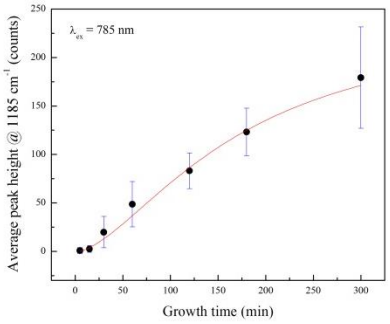
λex = 785 nm
Average peak height @ 1185 cm-1 (counts)
Growth time (min)

(d)

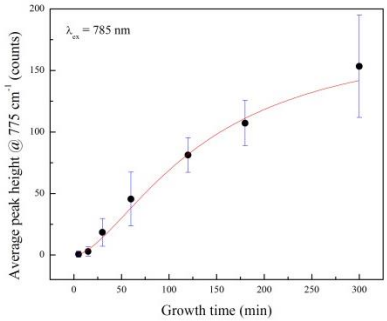
λex = 785 nm
Average peak height @ 775 cm-1 (counts)
Growth time (min)

(e)

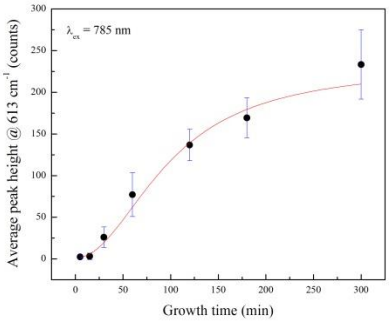
λex = 785 nm
Average peak height @ 613 cm-1 (counts)
Growth time (min)

Figure 4-10 Plots of the average peak height of Raman spectrum as a function of growth time at representative Raman shift band of Rh6G; (a) 1510 cm^{-1}, (b) 1365 cm^{-1}, (c) 1185 cm^{-1}, (d) 775 cm^{-1} and (e) 613 cm^{-1}.

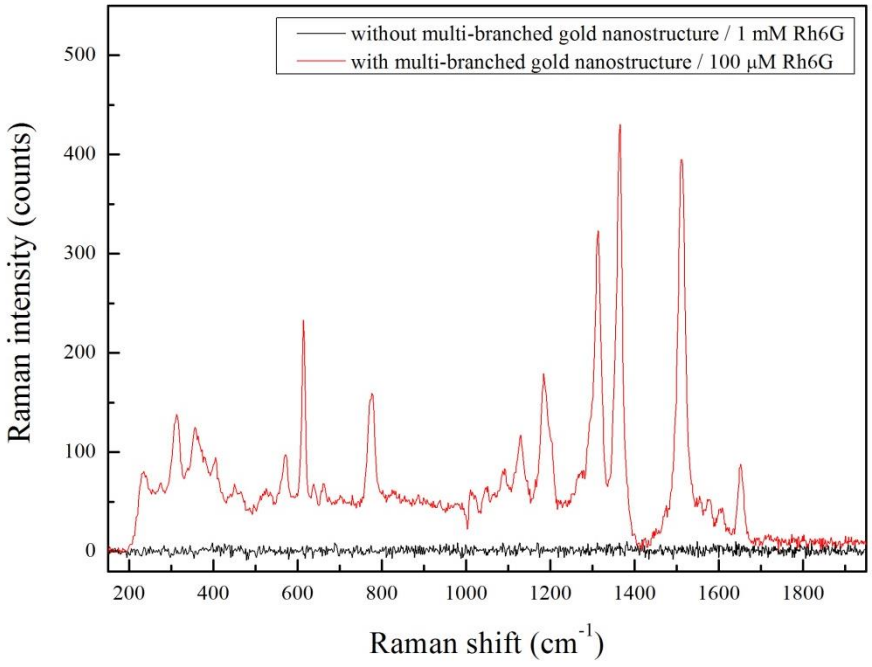

Figure 4-11 Comparison of Rh6G Raman spectrum with and without the multi-branched gold nanoparticle; nanostructure-immobilized substrate exposed to 100 μM Rh6G (red line), and clean substrate exposed to 1 mM Rh6G (black line)

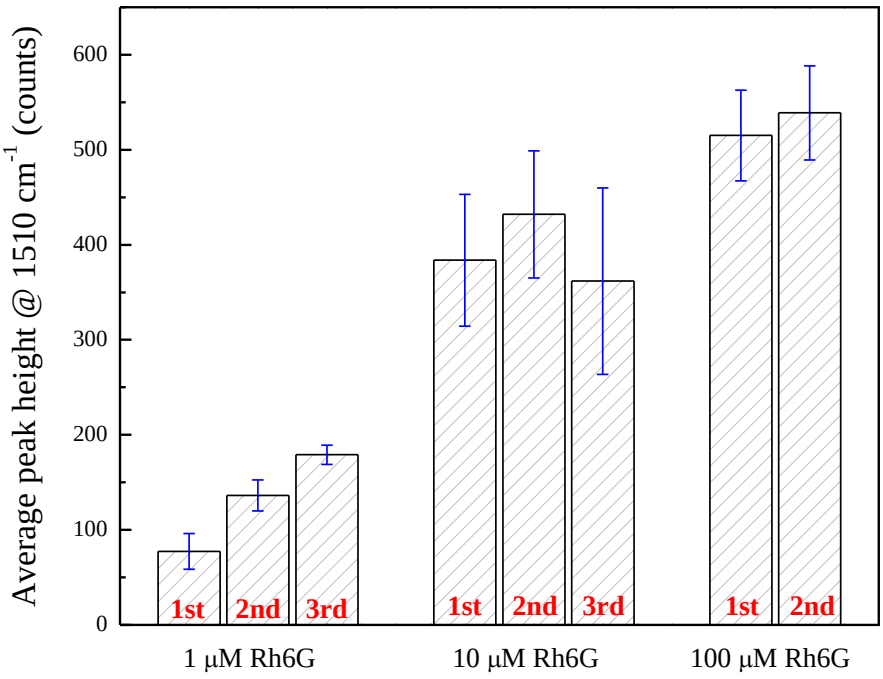

Figure 4-12 Change of average peak height at 1510 cm^{-1} with exposure to 1 μM, 10 μM and 100 μM Rh6G. Exposure to Rh6G and measurement of Raman spectrum were sequentially performed 3 times (with 1 μM, 10 μM Rh6G) or 2 times (with 100 μM) at each concentration. Each spectrum was collected 5 times with the randomly selected region, and averaged.

Chapter 5. Overall discussion

5.1 Biomimetic Sensor Chip for the Surface Plasmon Resonance

Highly specific interaction between a metal-deficient metalloenzyme and metal ion has been utilized in the selective detection of the metal ion by surface plasmon resonance spectroscopy (SPRS). SOD1 protein is a type of metalloprotein, which is consist of Cu and Zn as metal cofactors. Especially, Cu is directly involved in the catalytic activity of the enzyme, while Zn stabilizes the conformation of the protein. It means that E,Zn-SOD1 protein contains the specific site, where a Cu^{2+} ion selectively binds, thus maintaining its structure due to the role of Zn in its structure. By using the features of metal-deficient metalloenzyme, E,Zn-SOD1, I developed the highly selective detection system for Cu^{2+} ions by exploiting specific interactions between the E,Zn-SOD1 and Cu^{2+} ions using SPRS. It appears that metalloproteins have considerable potential for use as a novel sensing actuator, as evidenced by the selective binding of E,Zn-SOD1 proteins with Cu^{2+} ion. I believe that this approach can be used in conjunction with other fully or partially demetallated metalloproteins. Consequently, it could be potentially useful in the

determination of specific metal ions in aqueous media or demetallated proteins in biological fluids.

5.2 Plasmonic-based ratiometric sensor

The applicability of gold nanoparticles as a ratiometric sensor was suggested. Although metallic nanoparticles are well known as promising sensing probe compared to the organic materials due to the superior optical properties such as large light absorption / scattering cross-section and physic-chemical stability, there were almost no researches related with the ratiometric sensor using metallic nanoparticles. It is because that the metallic nanoparticles with typical shape mostly have one surface plasmon resonance (SPR) band, thus it is difficult to utilize two or more band for signal rationing.

From the theoretical study using discrete dipole approximation method, it is investigated that dimer structure of gold nanoparticles has unique optical properties compared to separated single gold nanoparticle. It can be appeared new plasmon band at longer wavelength due to the electron oscillations along the longitudinal interparticle axis, and the this band can be distinguished clearly with the inherent plasmon band.

Thus if the aggregation of gold nanoparticles induced by analyte can be limited to the dimer structure, the intensity ratio of inherent and additional plasmon band could be utilized as the value for the ratiometric sensor.

5.3 Metallic nanostructure for the Surface-enhanced Raman Active Substrate

Surface-enhanced Raman spectroscopy (SERS) is promising analytical tool for the sensitive and selective detection of molecules with extremely low concentration. The enhancement factor of Raman signal when using Raman active substrate can be understood as the product of two contributions [80];

(1) An electromagnetic enhancement mechanism and

(2) A chemical enhancement mechanism

In this research, I synthesized and characterized the multi-branched gold nanoparticles, which are applicable to the surface-enhanced Raman detection. It can be directly synthesized on the substrate with simple seed-mediated method, show the very high enhancement factor, thus it can be utilized as very effective SERS substrate. The features that can make them suitable for SERS substrates are as followed;

(1) Increased surface area due to their roughened surface determined by the tips and the cavities

(2) Contribution to the development of the so called ‘hot spot’ for localized electromagnetic field enhancement.

Bibliography

1. K. A. Willets, R. P. Van Duyne, *Annual Review of Physical Chemistry* **2007,** 58, (1), 267-297.
2. C. R. Yonzon, E. Jeoung, S. Zou, G. C. Schatz, M. Mrksich, R. P. Van Duyne, *Journal of the American Chemical Society* **2004,** 126, (39), 12669-12676.
3. B. Zhou, R. Li, Y. Zhang, Y. Liu, *Photochemical & Photobiological Sciences* **2008,** 7, (4), 453-459.
4. J. S. Yuk, J.-W. Jung, Y.-M. Kim, K.-S. Ha, *Sensors and Actuators B: Chemical* **2008,** 129, (1), 113-119.
5. J. Wang, R. Lv, J. Xu, D. Xu, H. Chen, *Analytical and Bioanalytical Chemistry* **2008,** 390, (4), 1059-1065.
6. M. d. Vestergaard, K. Kerman, D.-K. Kim, H. M. Hiep, E. Tamiya, *Talanta* **2008,** 74, (4), 1038-1042.
7. A. D. Taylor, J. Ladd, S. Etheridge, J. Deeds, S. Hall, S. Jiang, *Sensors and Actuators B: Chemical* **2008,** 130, (1), 120-128.
8. B. A. Sexton, B. N. Feltis, T. J. Davis, *Sensors and Actuators A: Physical* **2008,** 141, (2), 471-475.
9. Y. Sato, K. Hosokawa, M. Maeda, *Colloids and Surfaces B: Biointerfaces* **2008,** 62, (1), 71-76.
10. J. Ryu, H. A. Joung, M. G. Kim, C. B. Park, *Analytical Chemistry* **2008**.
11. R. L. Rich, M. J. Cannon, J. Jenkins, P. Pandian, S. Sundaram, R. Magyar, J. Brockman, J. Lambert, D. G. Myszka, *Analytical Biochemistry* **2008,** 373, (1), 112-120.

12. S. Natarajan, P. S. Katsamba, A. Miles, J. Eckman, G. A. Papalia, R. L. Rich, B. K. Gale, D. G. Myszka, *Analytical Biochemistry* **2008,** 373, (1), 141-146.
13. T. Mori, K. Inamori, Y. Inoue, X. Han, G. Yamanouchi, T. Niidome, Y. Katayama, *Analytical Biochemistry* **2008,** 375, (2), 223-231.
14. Y. Miao, T. Cui, F. Leng, W. D. Wilson, *Analytical Biochemistry* **2008,** 374, (1), 7-15.
15. A. Melikyan, H. Minassian, *Chemical Physics Letters* **2008,** 452, (1-3), 139-143.
16. K. M. Mayer, S. Lee, H. Liao, B. C. Rostro, A. Fuentes, P. T. Scully, C. L. Nehl, J. H. Hafner, *ACS Nano* **2008**.
17. T. Masadome, Y. Yano, T. Imato, *Analytical Letters* **2008,** 41, (4), 640 - 648.
18. M. G. Manera, J. Spadavecchia, A. Leone, F. Quaranta, R. Rella, D. Dell'atti, M. Minunni, M. Mascini, P. Siciliano, *Sensors and Actuators B: Chemical* **2008,** 130, (1), 82-87.
19. J.-T. Liu, L.-Y. Chen, M.-C. Shih, Y. Chang, W.-Y. Chen, *Analytical Biochemistry* **2008,** 375, (1), 90-96.
20. C. Caro, P. M. Castillo, R. Klippstein, D. Pozo, A. P. Zaderenko, Silver Nanoparticles: Sensing and Imaging Applications. In *Silver Nanoparticles*, Perez, D. P., Ed. InTech: 2010.
21. B. Vlckov, M. Moskovits, I. Pavel, K. Siskov, M. Sl?kov, M. Slouf, *Chemical Physics Letters* **2008,** 455, (4-6), 131-134.
22. S. Shanmukh, L. Jones, Y. P. Zhao, J. Driskell, R. Tripp, R. Dluhy, *Analytical and Bioanalytical Chemistry* **2008,** 390, (6), 1551-1555.
23. A. Sabur, M. Havel, Y. Gogotsi, *Journal of Raman Spectroscopy* **2008,** 39, (1), 61-67.

24. R. Narayanan, R. J. Lipert, M. D. Porter, *Analytical Chemistry* **2008,** 80, (6), 2265-2271.
25. B. L. Mitchell, A. J. Patwardhan, S. M. Ngola, S. Chan, N. Sundararajan, *Journal of Raman Spectroscopy* **2008,** 39, (3), 380-388.
26. J. R. Lombardi, R. L. Birke, *Journal of Physical Chemistry C* **2008,** 112, (14), 5605-5617.
27. X. Liu, S. Huan, Y. Bu, G. Shen, R. Yu, *Talanta* **2008,** 75, (3), 797-803.
28. Z. H. Lin, H. T. Chang, *Langmuir* **2008,** 24, (2), 365-367.
29. D.-F. Zhang, L.-Y. Niu, L. Jiang, P.-G. Yin, L.-D. Sun, H. Zhang, R. Zhang, L. Guo, C.-H. Yan, *The Journal of Physical Chemistry C* **2008,** 112, (41), 16011-16016.
30. F. Le, D. W. Brandl, Y. A. Urzhumov, H. Wang, J. Kundu, N. J. Halas, J. Aizpurua, P. Nordlander, *ACS Nano* **2008**.
31. L. Brus, *Accounts of Chemical Research* **2008**.
32. S. Basu, S. Jana, S. Pande, T. Pal, *Journal of Colloid and Interface Science* **2008,** 321, (2), 288-293.
33. A. Barhoumi, D. Zhang, F. Tam, N. J. Halas, *Journal of the American Chemical Society* **2008,** 130, (16), 5523-5529.
34. F. Bao, J. F. Li, B. Ren, J. L. Yao, R. A. Gu, Z. Q. Tian, *Journal of Physical Chemistry C* **2008,** 112, (2), 345-350.
35. N. A. Abu Hatab, J. M. Oran, M. J. Sepaniak, *ACS Nano* **2008,** 2, (2), 377-385.
36. M. Wang, N. Jing, I. H. Chou, G. L. Cote, J. Kameoka, *Lab on a Chip* **2007,** 7, (5), 630-632.
37. B. Vlckova, I. Pavel, M. Sladkova, K. Siskova, M. Slouf, *Journal of Molecular Structure* **2007,** 834-836, 42-47.

38. B. D. Piorek, S. J. Lee, J. G. Santiago, M. Moskovits, S. Banerjee, C. D. Meinhart, *Proceedings of the National Academy of Sciences of the United States of America* **2007,** 104, (48), 18898-18901.
39. E. C. LeRu, Blackie.E, M. Meyer, P. G. Etchegoin, *Journal of Physical Chemistry C* **2007,** 111, (37), 13794-13803.
40. S. J. Lee, Z. Guan, H. Xu, M. Moskovits, *Journal of Physical Chemistry C* **2007,** 111, (49), 17985-17988.
41. E. Kim, H. E. Kim, S. J. Lee, S. S. Lee, M. L. Seo, J. H. Jung, *Chemical Communications* **2008**, (33), 3921-3923.
42. J.-S. Lee, M. S. Han, C. A. Mirkin, *Angewandte Chemie International Edition* **2007,** 46, (22), 4093-4096.
43. X. F. Liu, Y. L. Tang, L. H. Wang, J. Zhang, S. P. Song, C. Fan, S. Wang, *Advanced Materials* **2007,** 19, (11), 1471-1474.
44. J. B. Wang, X. H. Qian, *Chemical Communications* **2006**, (1), 109-111.
45. S. Wang, E. S. Forzani, N. Tao, *Analytical Chemistry* **2007,** 79, (12), 4427-4432.
46. F. A. Settle, *Handbook of instrumental techniques for analytical chemistry*. Prentice Hall: New Jersey, 1997.
47. T. Dudev, C. Lim, *Annual Review of Biophysics* **2008,** 37, (1), 97-116.
48. A. Messerschmidt, R. Huber, K. Wieghardt, T. Poulos, *Handbook of Metalloproteins*. 1 ed.; John Wiley & Sons: New York, 2001.
49. J. A. Tainer, E. D. Getzoff, K. M. Beem, J. S. Richardson, D. C. Richardson, *Journal of Molecular Biology* **1982,** 160, (2), 181-217.
50. J. A. Tainer, E. D. Getzoff, J. S. Richardson, D. C. Richardson, *Nature* **1983,** 306, (5940), 284-287.
51. G. Rotilio, L. Calabrese, F. Bossa, D. Barra, A. F. Agro, B. Mondovi, *Biochemistry* **1972,** 11, (11), 2182-2187.

52. T. Kang, S. Hong, I. Choi, J. J. Sung, Y. Kim, J. S. Hahn, J. Yi, *Journal of the American Chemical Society* **2006,** 128, (39), 12870-12878.
53. B. L. Frey, R. M. Corn, *Analytical Chemistry* **1996,** 68, (18), 3187-3193.
54. J. Y. Zhou, P. Prognon, *Journal of Pharmaceutical and Biomedical Analysis* **2006,** 40, (5), 1143-1148.
55. B. Zhu, X. Zhang, H. Jia, Y. Li, H. Liu, W. Tan, *Organic & Biomolecular Chemistry* **2010,** 8, (7), 1650-1654.
56. Z. Xu, J. Yoon, D. R. Spring, *Chemical Communications* **2010,** 46, (15), 2563-2565.
57. C. Jia, B. Wu, J. Liang, X. Huang, X.-J. Yang, *Journal of Fluorescence* **2010,** 20, (1), 291-297.
58. Z.-X. Han, X.-B. Zhang, Z. Li, Y.-J. Gong, X.-Y. Wu, Z. Jin, C.-M. He, L.-X. Jian, J. Zhang, G.-L. Shen, R.-Q. Yu, *Analytical Chemistry* **2010,** 82, (8), 3108-3113.
59. X. Cheng, Q. Li, J. Qin, Z. Li, *ACS Applied Materials & Interfaces* **2010,** 2, (4), 1066-1072.
60. H.-H. Wang, L. Xue, Y.-Y. Qian, H. Jiang, *Organic Letters* **2009,** 12, (2), 292-295.
61. H. Li, H. Yan, *The Journal of Physical Chemistry C* **2009,** 113, (18), 7526-7530.
62. Z. Xu, J. Pan, D. R. Spring, J. Cui, J. Yoon, *Tetrahedron* **2010,** 66, (9), 1678-1683.
63. D. Srikun, E. W. Miller, D. W. Domaille, C. J. Chang, *Journal of the American Chemical Society* **2008,** 130, (14), 4596-4597.
64. H. Yang, Z.-Q. Liu, Z.-G. Zhou, E.-X. Shi, F.-Y. Li, Y.-K. Du, T. Yi, C.-H. Huang, *Tetrahedron Letters* **2006,** 47, (17), 2911-2914.

65. Z. Xu, Y. Xiao, X. Qian, J. Cui, D. Cui, *Organic Letters* **2005,** 7, (5), 889-892.
66. Z. Xu, X. Qian, J. Cui, *Organic Letters* **2005,** 7, (14), 3029-3032.
67. E. G. Matveeva, Z. Gryczynski, D. R. Stewart, I. Gryczynski, *Journal of Luminescence* **2010,** 130, (4), 698-702.
68. G.-Q. Shang, X. Gao, M.-X. Chen, H. Zheng, J.-G. Xu, *Journal of Fluorescence* **2008,** 18, (6), 1187-1192.
69. H. J. Kim, S. Y. Park, S. Yoon, J. S. Kim, *Tetrahedron* **2008,** 64, (7), 1294-1300.
70. A. E. Albers, V. S. Okreglak, C. J. Chang, *Journal of the American Chemical Society* **2006,** 128, (30), 9640-9641.
71. H. S. Jung, M. Park, D. Y. Han, E. Kim, C. Lee, S. Ham, J. S. Kim, *Organic Letters* **2009,** 11, (15), 3378-3381.
72. H. M. Hiep, T. Endo, M. Saito, M. Chikae, D. K. Kim, S. Yamamura, Y. Takamura, E. Tamiya, *Analytical Chemistry* **2008,** 80, (6), 1859-1864.
73. J. Yguerabide, E. E. Yguerabide, *Analytical Biochemistry* **1998,** 262, (2), 157-176.
74. J. Yguerabide, E. E. Yguerabide, *Analytical Biochemistry* **1998,** 262, (2), 137-156.
75. B. T. Draine, P. J. Flatau, *J. Opt. Soc. Am. A* **1994,** 11, (4), 1491-1499.
76. B. T. Draine, P. J. Flatau User Guide to the Discrete Dipole Approximation Code DDSCAT 7.2. http://arXiv.org/abs/1202.3424
77. M. G. Albrecht, J. A. Creighton, *Journal of the American Chemical Society* **1977,** 99, (15), 5215-5217.
78. M. Fleischmann, P. J. Hendra, A. J. McQuillan, *Chemical Physics Letters* **1974,** 26, (2), 163-166.

79. D. L. Jeanmaire, R. P. Van Duyne, *Journal of Electroanalytical Chemistry and Interfacial Electrochemistry* **1977,** 84, (1), 1-20.
80. P. L. Stiles, J. A. Dieringer, N. C. Shah, R. P. Van Duyne, *Annual Review of Analytical Chemistry* **2008,** 1, (1), 601-626.
81. K. D. Alexander, K. Skinner, S. Zhang, H. Wei, R. Lopez, *Nano Letters* **2010,** 10, (11), 4488-4493.
82. X. Hu, W. Cheng, T. Wang, Y. Wang, E. Wang, S. Dong, *The Journal of Physical Chemistry B* **2005,** 109, (41), 19385-19389.
83. C. J. Orendorff, L. Gearheart, N. R. Jana, C. J. Murphy, *Physical Chemistry Chemical Physics* **2006,** 8, (1), 165-170.
84. R. Sancı, M. Volkan, *Sensors and Actuators B: Chemical* **2009,** 139, (1), 150-155.
85. S. Barbosa, A. Agrawal, L. Rodríguez-Lorenzo, I. Pastoriza-Santos, R. n. A. Alvarez-Puebla, A. Kornowski, H. Weller, L. M. Liz-Marzán, *Langmuir* **2010,** 26, (18), 14943-14950.
86. F. Hao, C. L. Nehl, J. H. Hafner, P. Nordlander, *Nano Letters* **2007,** 7, (3), 729-732.
87. C. L. Nehl, H. Liao, J. H. Hafner, *Nano Letters* **2006,** 6, (4), 683-688.
88. D. Senapati, A. K. Singh, S. A. Khan, T. Senapati, P. C. Ray, *Chemical Physics Letters* **2011,** 504, (1–3), 46-51.
89. Q. Su, X. Ma, J. Dong, C. Jiang, W. Qian, *ACS Applied Materials & Interfaces* **2011,** 3, (6), 1873-1879.
90. H.-L. Wu, C.-H. Chen, M. H. Huang, *Chemistry of Materials* **2008,** 21, (1), 110-114.
91. H. Liang, Z. Li, W. Wang, Y. Wu, H. Xu, *Advanced Materials* **2009,** 21, (45), 4614-4618.

92. W. Wang, X. Yang, H. Cui, *The Journal of Physical Chemistry C* **2008,** 112, (42), 16348-16353.
93. J. Xie, Q. Zhang, J. Y. Lee, D. I. C. Wang, *ACS Nano* **2008,** 2, (12), 2473-2480.
94. L. Ming, K. C. Scott, Z. Jianming, L. Jessica, P. A. Zoraida, M. Dongling, W. Nianqiang, *Nanotechnology* **2012,** 23, (11), 115501.
95. J. A. Sanchez-Gil, J. V. Garcia-Ramos, *The Journal of Chemical Physics* **1998,** 108, (1), 317-325.
96. Y. Weisheng, Y. Yang, W. Zhihong, H. Jiaguang, S. Ahad, C. Longqing, W. Kimchong, W. Xianbin, *Journal of Physics D: Applied Physics* **2012,** 45, (42), 425401.
97. S. J. Lee, A. R. Morrill, M. Moskovits, *Journal of the American Chemical Society* **2006,** 128, (7), 2200-2201.
98. X. Huang, I. H. El-Sayed, W. Qian, M. A. El-Sayed, *Journal of the American Chemical Society* **2006,** 128, (6), 2115-2120.
99. H. D. Song, I. Choi, Y. I. Yang, S. Hong, S. Lee, T. Kang, J. Yi, *Nanotechnology* **2010,** 21, (14), 145501.
100. A. Y. Panarin, S. N. Terekhov, K. I. Kholostov, V. P. Bondarenko, *Applied Surface Science* **2010,** 256, (23), 6969-6976.
101. P. Hildebrandt, M. Stockburger, *The Journal of Physical Chemistry* **1984,** 88, (24), 5935-5944.
102. Liu, P. Guyot-Sionnest, *The Journal of Physical Chemistry B* **2005,** 109, (47), 22192-22200.
103. T. Ming, W. Feng, Q. Tang, F. Wang, L. Sun, J. Wang, C. Yan, *Journal of the American Chemical Society* **2009,** 131, (45), 16350-16351.
104. J. Zhang, M. R. Langille, M. L. Personick, K. Zhang, S. Li, C. A. Mirkin, *Journal of the American Chemical Society* **2010,** 132, (40), 14012-14014.

105. S. K. Dondapati, T. K. Sau, C. Hrelescu, T. A. Klar, F. D. Stefani, J. Feldmann, *ACS Nano* **2010,** 4, (11), 6318-6322.

국문초록

나노과학, 의료, 환경 등 여러 과학 분야에서, 특정 목적에 부합하는 형태의 나노구조체를 설계 및 제조하는 것은 매우 중요하다. 특히 금속성 나노구조체는 화학 센서의 분야에서 상당한 주목을 받고 있는데, 이는 금속성 나노구조체가 가지는 물리화학적 우수성 뿐 아니라 표면플라즈몬 공명 현상을 다양한 방법으로 응용할 수 있기 때문이다. 이 학위논문은 금속성 나노입자의 표면플라즈몬공명 현상을 응용한 여러 형태의 화학적 센서의 구현에 대해 다루고 있다. 이와 관련된 연구의 배경 및 세부 결과에 대한 요약은 다음과 같다;

첫째, 탈금속화된 금속단백질과 금속이온 사이에서의 상호작용을 응용하여, 표면 플라즈몬 공명 분석에 응용할 수 있는 높은 선택도의 금속이온 센서를 제안하였다. 구리가 탈금속화된 수퍼옥사이드 디스뮤타제의 경우, 탈금속화된 위치에서 다른 이가 금속이온과 비교해 구리이온에 대한 높은 친화도를 나타내는 것을 확인하였다. 이러한 특성을 표면플라즈몬공명 분석법에 응용하여,

저농도의 구리를 선택적으로 검출할 수 있는 센서칩을 제작하고 그 성능을 평가하였다. 이러한 금속단백질의 응용은, 수퍼옥사이드 디스뮤타제와 같은 기타의 금속단백질에도 동일한 원리로 적용 가능하며, 수중에서의 다양한 금속이온 검출을 위한 효율적 센서의 개발에 응용될 수 있다.

둘째, 이합체 형태의 금속성 나노입자에 대한 광학적 성질을 이론적 모사 방법으로 확인하였으며, 비율계량식 센서에의 응용 가능성에 대해 제안하였다. 특히 이합체 형태의 금나노입자가 특이한 광학적 성질을 가짐을 이산쌍극자근사 계산법을 이용하여 확인하였으며, 입자간 장축 에서의 특이적 전자진동에 의해 기존의 플라즈몬 밴드 외에 새로운 플라즈몬 밴드가 형성이 됨을 보였다. 명확히 구분될 수 있는 두개의 플라즈몬 밴드는 단일체/이합체의 비율에 따라 각 밴드의 세기가 달라지게 되며, 이러한 원리를 적용하여 금속성 나노입자를 기반으로 하는 비율계량식 센서가 구현 가능함을 이론적으로 확인하였다.

마지막으로, 간단한 방법으로 꽃잎 모양의 팁을 가지는 3 차원 금나노구조체를 기판 위에에서 바로 형성시키는 기법을 제안하였다. 기존의 많은 연구에서 복잡한 형태의 금나노구조체의 경우 풍부한

‘핫스팟’으로 인해 매우 강한 전자기장을 형성하는 것으로 보고되었다. 높은 감도의 표면증강라만 분석에 응용하기 위해, 다중갈래형태의 금나노구조체를 제안하였으며 간단한 방법으로 기판 상에서 바로 성장시켜 제작하였다. 제조된 다중갈래형태의 금나노구조체는 그 성장과정을 모양 변화 및 광학적 특성 변화로 확인 하였으며, 표면증강라만 분석을 통해 매우 강한 표면 증강 효과를 가짐을 확인하였다.

주요어: 표면플라즈몬공명, 비율계량식센서, 이산쌍극자근사, 생체모방형 센서, 금속단백질, 금속나노구조체, 표면증강라만분석

학번: 2008-30894

List of publications

- International Academic Published Papers

1. **S. Lee**, I. Choi, S. Hong, Y. I. Yang, J. Lee, T. Kang, and J. Yi, Highly Selective Detection of Cu^{2+} Utilizing Specific Binding between Cu-demetallated Superoxide Dismutase 1 and Cu^{2+} ion via Surface Plasmon Resonance Spectroscopy, Chemical Communications, 41, 6171-6173 (2010)

2. **S. Lee**, C. Y. Yun, M. S. Hahn, J. Lee and J. Yi, Synthesis and Characterization of Carbon-Doped Titania as a Visible-Light-Sensitive Photocatalyst, Korean Journal of Chemical Engineering, 25(4), 892-896 (2008)

3. M. Eo*, J. Baek*, H. D. Song, **S. Lee**, and J. Yi (*co-first author), Quantification of electron transfer rates of different facets on single gold nanoparticles during catalytic reaction, Chemical Communications, 49(45), 5204-5206 (2013)

4. S. Park, E. H. Kim, M. Eo, H. D. Song, **S. Lee**, J.-K. Roh, B.-C. Lee, Y. Kim, and J. Yi, Effect of Dispersion Stability on the

Deposition of Citrate-Capped Silver Nanoparticles in Natural Soils, Journal of Nanoscience and Nanotechnology, 13(3), 2224-2229 (2013)

5. S. Hong, **S. Lee**, I. Choi, Y. I. Yang, T. Kang, and J. Yi, Real-time analysis and direct observations of different superoxide dismutase (SOD1) molecules bindings to aggregates in temporal evolution step, Colloids and Surfaces B: Biointerfaces, 101, 266-271 (2013)

6. I. Choi*, H. D. Song*, **S. Lee**, Y. I. Yang, T. Kang, and J. Yi (*co-first author), Core-Satellites Assembly of Silver Nanoparticles on a Single Gold Nanoparticle via Metal Ion-mediated Complex, Journal of the American Chemical Society, 134(29), 12083-12090 (2012)

7. I. Choi, H. D. Song, **S. Lee**, Y. I. Yang, J. H. Nam, S. J. Kim, J. J. Sung, T. Kang, and J. Yi, Direct Observation of Defects and Increased Ion Permeability of a Membrane Induced by Structurally Disordered Cu/Zn-Superoxide Dismutase Aggregates, PLoS ONE, 6(12), e28982: 1-10 (2011)

8. S. Hong, **S. Lee**, and J. Yi, Sensitive and Molecular Size-Selective Detection of Proteins Using a Chip-based and Heteroliganded Gold Nanoisland By Localized Surface Plasmon Resonance Spectroscopy, Nanoscale Research Letters, 6, 336-342 (2011)

9. Y. I. Yang*, E. Jeong*, I. Choi, **S. Lee**, H. D. Song, K. Kim, Y. Choi, T. Kang, and J. Yi (* co-first author), Simultaneous Optical Monitoring of the Overgrowth Modes of Individual Asymmetric Hybrid Nanoparticles, Angewandte Chemie International Edition, 50(20), 4633-4636 (2011)

10. S. Hong, S. Park, **S. Lee**, Y. I. Yang, H. D. Song, and J. Yi, The Sensitive, Anion-Selective Detection of Arsenate with Poly(allylamine hydrochloride) By Single Particle Plasmon-Based Spectroscopy, Analytica Chimica Acta, 694(1), 136-141 (2011)

11. I. Choi, Y. I. Yang, H. D. Song, J. **S. Lee**, T. Kang, J.-J. Sung, and J. Yi, Lipid molecules induce the cytotoxic aggregation of Cu/Zn superoxide dismutase with structurally disordered regions,

Biochimica et Biophysica Acta - Molecular Basis of Disease , 1812(1), 41-48 (2011)

12. H. D. Song*, I. Choi*, Y. I. Yang, S. Hong, **S. Lee**, T. Kang, and J. Yi (* co-first author), Picomolar Selective Detection of Mercuric Ion (Hg^{2+}) Using a Functionalized Single Plasmonic Gold Nanoparticle, Nanotechnology, 21(14), 145501:1-6 (2010)

13. Y. I. Yang, I. Choi, S. Hong, **S. Lee**, T. Kang, H. Lee, and J. Yi, Selective Aggregation of Polyanion-Coated Gold Nanorods Induced by Divalent Metal Ions in an Aqueous Solution, Journal of Nanoscience and Nanotechnology, 10(5), 3538-3542 (2010)

14. S. Jeon, U. S. Kim, W. Jeon, S. Hong, I. Choi, **S. Lee**, J. Yi, and C. B. Shin, Fabrication of Multicomponent Protein Microarrays with Microfluidic Devices of Poly(dimethylsiloxane), Macromolecular Research, 17(3), 192-196 (2009)

15. S. Hong, I. Choi, **S. Lee**, Y. I. Yang, T. Kang, and J. Yi, Sensitive and colorimetric detection of the structural evolution of superoxide dismutase (SOD1) with gold nanoparticles, Analytical Chemistry, 81(4), 1378-1382 (2009)

16. I. Choi, Y. Kim, J. H. Kim, Y. I. Yang, J. Lee, **S. Lee**, S. Hong, and J. Yi, Fast image scanning method in liquid-AFM without image distortion, Nanotechnology, 19(44), 445701:1-8 (2008)

17. J. Lee, I. Choi, S. Hong, S. **S. Lee**, Y. I. Yang, Y. Kim and J. Yi, Construction of pcAFM module to measure photoconductance with a nanoscale spatial resolution, Ultramicroscopy, 108(10), 1090-1093 (2008)

- Papers in preparation

1. **S. Lee***, Y. I. Yang*, H. D. Song, and J. Yi (*co-first author), Multi-branched nanostructures for surface-enhanced Raman spectroscopy (SERS), **in preparation**

- Registered patents

1. 이종협, 양영인, 최인희, 송현돈, 홍수린, 이수승, 강태욱, 이현주, 단일 금 나노입자를 이용한 중금속 이온의 고감도 검출 센서, 특허 제 10-1117236 호 (2012.02.09) (특허 출원 10-2009-0025085 호, 2009.03.24)

2. 이종협, 홍수린, 이수승, 최인희, 양영인, 이중환, 유규상, 표면 플라즈몬 공명 장치를 이용한 수은 이온 검출용 DNA 기반 바이오센서, 특허 제 10-1015434 호 (2011.02.10) (특허 출원 10-2009-0011836 호, 2009.02.13)

3. 이종협, 최인희, 김영훈, 김종호, 양영인, 이정진, 이수승, 홍수린, 액상 조건에서의 초고속 원자간력 현미경

이미징 방법, 특허 제 10-1004966 호 (2010.12.23) (특허 출원 2009-0005171 호, 2009.01.21)

4. 이종협, 홍수린, 최인희, 이수승, 이중환, 유규상, 금 나노 입자를 이용하여 응집된 단백질을 검출하기 위한 바이오센서, 특허 제 10-0958184 호 (2010.05.07) (특허 출원 10-2008-0028970 호, 2008.03.28)

- Applied patents

1. 이종협, 송현돈, 최인희, 양영인, 이수승, 강태욱, 중심-위성 나노구조체의 플라즈몬 공명을 이용한 고감도 중금속 검출 센서 및 검출 방법, 특허 출원 10-2011-0071024 (2011.07.18)

2. 이종협, 이수승, 최인희, 양영인, 이정진, 강태욱, 표면 플라즈몬 공명 장치를 이용한 중금속 이온 검출용 금속 단백질 기반 바이오센서, 특허 출원 10-2009-0046014 (2009.05.26)

- International Conferences

1. **S. Lee**, I. Choi, S. Hong, Y. I. Yang, J. Lee, H.-D. Song, T. Kang, and J. Yi, Biomimetic Sensors for the Heavy Metal Detection, The 8th Annual IEEE Conference on Sensors, Christchurch Convention Centre, Christchurch, New Zealand, Oct. 25-28 (2009)

2. **S. Lee**, J. Lee, Y. Kim, K. Park, J. W. Lee, M. B. Gu, D. Y. Ryu, and J. Yi, Evaluation of In vitro effect of nanoparticles on proteins, The 7th International Symposium on Advanced Environmental Monitoring, East-West Center Honolulu, HI, USA, Feb. 25-28 (2008)

3. **S. Lee**, J. Lee, I. Choi, S. Hong, Y. I. Yang, Y. Kim and J. Yi, Preparation and application of visible-light responsive TiO2 photocatalyst for organic pollutant degradation, NSTI Nanotech 2007, Santa Clara Convention Center, Santa Clara, USA, May 20-24 (2007)

- Domestic Conferences

1. **이수승**, 양영인, 송현돈, 어문정, 이종협, 유기-무기 복합나노입자를 이용한 분광학적 센서의 개발, 한국환경분석학회 춘계학술대회, STX 리조트, 5. 24-25 (2012)

2. **이수승**, 김기훈, 양영인, 어문정, 송현돈, 박수민, 강태욱, 이종협, 금속성 나노입자 기반의 분광 센서 탐침자 개발, 추계 환경분석학회, 제주 KAL 호텔, 11. 24-25 (2011)

3. **이수승**, 정선일, 정의근, 홍수린, 양영인, 송현돈, 최인희, 강태욱, 이종협, Bimetallic core-satellites single nanoprobe for the detection of Pb^{2+} ion, 춘계화학공학회, 대구 EXCO, 4. 21-23 (2010)

4. **이수승**, 최인희, 홍수린, 양영인, 강태욱, 유규상, 구수진, 이종협, 표면플라즈몬공명을 이용하는 새로운 중금속 이온 검출 기법, 춘계화학공학회, 김대중컨벤션센터, 광주, 4.22-24 (2009)

5. **이수승**, 최인희, 홍수린, 양영인, 강태욱, 유규상, 구수진, 이종협, Metalloprotein-based surface plasmon resonance sensor for the selective detection of Cu^{2+} ions in an aqueous solution, 추계화학공학회, BEXCO, 부산, 10.22-24 (2008)

6. **이수승**, 이정진, 배은주, 곽병규, 김영훈, 이종협, 은나노입자의 Toxicity 연구, 한국환경분석학회, 서울대학교 ICP, 5.22-23 (2008)

7. **이수승**, 홍수린, 최인희, 양영인, 강태욱, 이종협, Metalloprotein 기반의 센서칩 개발과 표면플라즈몬공명 분광기를 이용한 중금속의 선택적 검출에의 활용, 한국청정기술학회, 고려대학교, 5.23 (2008)

8. **이수승**, 이정진, 배은주, 최인희, 홍수린, 양영인, 김영훈, 이종협, The effects of silver nanoparticles on Cu/Zn-superoxide dismutase (SOD1) human protein, 한국화학공학회, 제주 ICC, 4.23-25 (2008)

9. **이수승**, 이정진, 배은주, 최인희, 홍수린, 양영인, 곽병규, 김영훈, 이종협, 표면 플라즈몬 공명을 이용한 환경/인체

잠재위해성 나노입자와 단백질간의 상호작용 분석, 한국환경분석학회, 부경대학교, 11.22-23 (2007)

10. **이수승**, 이정진, 배은주, 최인희, 홍수린, 양영인, 김영훈, 이종협, In vitro Effect of Silver Nanoparticles on Superoxide dismutase (SOD), 추계화학공학회, 한국과학기술원, 10. 26-27 (2007)

11. **이수승**, 이정진, 최인희, 홍수린, 양영인, 김영훈, 이종협, SPR (Surface Plasmon Resonance) signal enhancement for the VOCs detection of ambient air using Au nanoparticles, 춘계화학공학회, 울산 롯데호텔, 4. 19-20 (2007)

12. **이수승**, 이정진, 김진수, 이종협, 화학적으로 개질된 이산화티타늄 광촉매의 제조 및 특성분석, 추계청정기술학회, 수원대학교, 11.17 (2006)

13. **이수승**, 김진수, 이정진, 김영훈, 이종협, 탄소와 질소가 도핑된 이산화티타늄(TiO_2) 광촉매의 특성분석 및 광분해 효과, 추계화학공학회, 고려대학교, 10.27-28 (2006)

14. **이수승**, 김진수, 윤창연, 이종협, 견운모와 규조토의 기공 특성에 따른 암모니아 기체 흡착 특성, 춘계청정기술학회, 연세대학교, 5. 19 (2006)

15. **이수승**, 김진수, 윤창연, 이종협, 화학적으로 개질된 이산화티타늄(TiO_2)의 상태밀도(Density of States) 전산모사, 춘계화학공학회, 대구 인터불고호텔, 4. 20-21 (2006)